minerals

MDPI

Article

Egyptian Blue Pellets from the First Century BCE Workshop of Kos (Greece): Microanalytical Investigation by Optical Microscopy, Scanning Electron Microscopy-X-ray Energy Dispersive Spectroscopy and Micro-Raman Spectroscopy

Ariadne Kostomitsopoulou Marketou [1,*], Fabrizio Andriulo [2], Calin Steindal [2] and Søren Handberg [1]

[1] Department of Archaeology, Conservation and History, University of Oslo, Blindernveien 11, 0371 Oslo, Norway; soren.handberg@iakh.uio.no

[2] SciCult Laboratory, Department of Collection Management, Museum of Cultural History, University of Oslo, St. Olavs Plass, 0130 Oslo, Norway; fabrizio.andriulo@khm.uio.no (F.A.); c.c.steindal@khm.uio.no (C.S.)

* Correspondence: a.k.marketou@iakh.uio.no; Tel.: +47-485-04-187

Received: 28 October 2020; Accepted: 23 November 2020; Published: 27 November 2020

Abstract: This paper aims to expand our understanding of the processes involved in the production of the artificial pigment Egyptian blue through the scientific examination of pigments found in the first century BCE workshop of the Greek island of Kos. There, 136 Egyptian blue pellets were brought to light, including successfully produced pellets, as well as partially successful and unsuccessful products. This study is based on the examination of eighteen samples obtained from pellets of various textures and tones of blue, including light and dark blue pigments, coarse and fine-grained materials, and one unsuccessful pellet of dark green/grey colour. The samples were examined by optical microscopy, scanning electron microscopy coupled with energy-dispersive X-ray spectroscopy (SEM-EDS), and micro-Raman spectroscopy. These complementary microanalytical techniques provide localised information about the chemical and mineralogical composition of this multicomponent material, at a single-grain level. The results shed light on the firing procedure and indicate possible sources for raw materials (beach sand, copper alloys), as well as demonstrating the use of a low-alkali starting mixture. Moreover, two different process for the production of light blue pigments were identified: (a) decreased firing time and (b) grinding of the initially produced pellet and mixing with cobalt-containing material.

Keywords: Egyptian blue; ancient production technology; pigments; Kos; Graeco-Roman art; micro-Raman; SEM-EDS

1. Introduction

Egyptian blue is an artificial material that, since its invention in the third millennium BCE, was used extensively as a blue pigment across the ancient Mediterranean world [1,2]. This remarkably stable blue pigment was suitable for outdoor use [3,4] since, unlike azurite, it could resist the harsh alkali conditions of fresco paintings. The material found various applications and was the main blue pigment throughout antiquity [1–3,5,6].

The blue pigment's name, Egyptian blue, can be traced back to the fourth century BCE writings of Theophrastus, who describes it as "manufactured, such as the one in Egypt" ("σκευαστὸς ὥσπερ ἐν Αἰγύπτῳ" in the original text) [7], signifying the origin of the material. However, Egyptian blue was used far beyond Egypt. Early examples that testify to the widespread use of Egyptian blue are the Bronze Age wall paintings of Thera [8], Knossos [9], and Mycenae [10]. Its usage in the Aegean was particularly favoured during the Late Bronze Age (16th to 12th century BCE), with numerous beads and inlays found in tombs [11]. Later characteristic examples of the use of Egyptian blue are the polychrome Archaic statues from the Athenian Acropolis [12], the decorations of architectural elements of the Parthenon temple and the ceiling of the Tower of the Winds in Athens [13]. Moreover, the blue pigments in the richly decorated Macedonian tombs of the Hellenistic period were identified as Egyptian blue [14,15]. The pigment has also been identified in Etruscan [16] and Roman art [1,17–24], with nearly all of the samples studied by S. Augusti from Pompeii identified as Egyptian blue [25]. Archaeological research has unearthed countless works of art that testify to the use of Egyptian blue, even as far north as in Norway [26], with the mentioned examples demonstrating the wide temporal and geographic use of the material. Besides its application as a pigment, the material could be moulded and has thus been used for the manufacture of beads, scarabs, and even mosaic tesserae in different historical periods [1,3,6,27,28].

Archaeological evidence suggests that during Hellenistic and Roman times, which witnessed an increased need for pigments for wall paintings, the demand for Egyptian blue rose [1]. However, despite the numerous archaeological finds that demonstrate the broad applications of Egyptian blue, material evidence of Egyptian blue production is scarce [29]. In the Graeco-Roman world, it has been suggested that Egyptian blue manufacturing sites can be identified in Memphis in Egypt [17,30,31] and Cumae, Liternum, and Puteoli in central Italy [32–34]. In addition to these possible production sites, evidence for late Hellenistic (first century BCE) Egyptian blue production was brought to light through the excavations of the Greek Archaeological Service on the Aegean island of Kos, under the scientific supervision of Ch. Kantzia [35].

The Koan workshop is located in a rear room of a stoa building at the east border of the agora of Kos (Figure 1). There, 136 Egyptian blue raw pigment finds were unearthed, including pellets of a saturated blue colour, finely ground material, pellets of lighter blue tones, as well as partially successful pellets and unsuccessful products, on the surface of which blue is only visible in few areas, if present at all [36]. The majority of the pellets, including both successful and unsuccessful products, were found in the context of a fire structure (FS 1 in Figure 1) [36]. Besides Egyptian blue production, archaeological evidence suggests that metallurgical activities, related to lead metallurgy, and the treatment of earth pigments were also carried out at the same workshop [35–37].

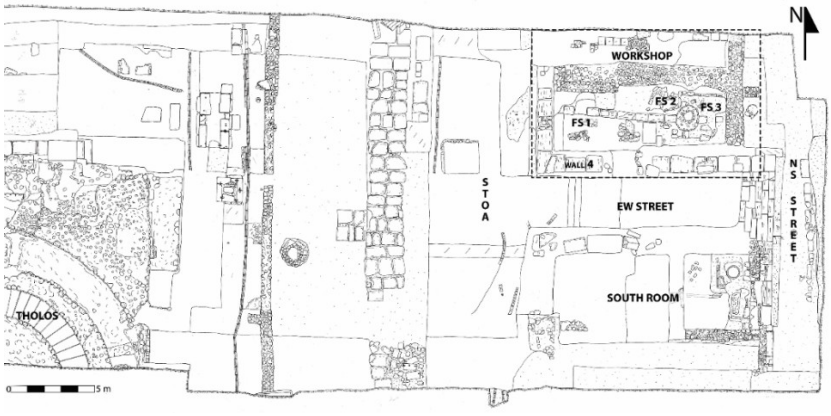

Figure 1. Plan of the excavated site with the location of the workshop and its surroundings; adapted after E. Tsampouniari (drawing), Ch. Kantzia, and E. Papanikolaou (archaeological survey). Image: courtesy of the

Ephorate of Antiquities of the Dodecanese. The workshop is located in one of the rear rooms of the agora's east stoa. Most of the Egyptian blue pellets (98 out of 136) were found in the context of a destroyed fire structure (indicated by FS1 on the plan).

Several previous studies have focused on the physicochemical characterisation of Egyptian blue from different contexts to shed light on the complex pyrotechnological process employed for its production [6,17,27,38–50]. Based on these studies, it is now known that the synthesis of Egyptian blue requires a silica source, most commonly quartz sand, a copper source, either copper alloys, metallic copper or copper ores, and a calcium compound, which could either be intentionally added or naturally present in the sand used for the production. These starting materials were finely ground and fired at temperatures ranging from 850 to 1050 °C. To ensure the synthesis of the material with the firing temperatures achievable in antiquity, an alkali flux, most commonly plant ashes or natron, had to be added to the starting mixture. The firing of Egyptian blue was a demanding process that required an oxidising atmosphere and took several hours.

The final product is a multicomponent material, and its characteristic saturated blue colour is mainly attributed to the Cu^{2+} ions from the copper-calcium-tetrasilicate crystals, which are formed during the synthesis of the material [38,45,51]. These crystals, also referred to as Egyptian blue crystals, are the synthetic equivalent to the naturally occurring mineral cuprorivaite ($CaCuSi_4O_{10}$) [52–54]. Besides cuprorivaite, previous research has demonstrated the presence of several other mineral phases in Egyptian blue, namely unreacted quartz and glassy phases [27,39,41,45–47]. Questions regarding the use of raw materials, the firing processes and temperatures, as well as the secondary treatment of the material, have previously been approached by the chemical and mineralogical analysis of Egyptian blue samples from different sites [1,6,17,27,34,41,43,45,48,49,55].

The presence of both successfully and unsuccessfully produced Egyptian blue pellets in the context of the Koan workshop provides a unique opportunity to compare the technological processes and choices involved in the manufacture of this artificial blue material. Moving beyond the initial classification of successfully and unsuccessfully produced pellets, the presence of which suggests the in situ production of Egyptian blue [35,36], a variation in terms of shade is readily observable among the blue pigments of the Koan workshop (Figure 2). The so-called successfully produced pellets can, therefore, be qualitatively placed on a scale based on their tone and texture, which ranges from dark to light blue and from coarse to fine-grained (see Figure 2 and Table 1). Such variations in the shade of Egyptian blue finds have also been documented in the raw pigment lumps from Pompeii, studied by Augusti and Delamare [25,55].

Pliny the Elder, in his accounts on pigments and their prices in the first century CE, elaborates on the production, uses, and prices of *caerulei* (i.e., blue pigments) (Plin. *HN* 33.162-163) [56]. Pliny informs us about four types of blue pigments: *caeruleum* (8 denarii/pound), *lomentum* (10 denarii/pound), *caeruleum Vestorianum* (11 denarii/pound), *Puteolani* or *cyanos* (possibly other names for *Vestorianum*), *Indicum (*7 denarii/pound*)*, and ground *lomentum* (5 asses/pound) (Plin. *HN* 33.162-163) [56]. The range of prices suggests a variation in terms of the quality, the production process, and/or the intended uses of these materials [1,55].

Which of these blue pigments described by Pliny can be considered products deriving from the processing of Egyptian blue? The Latin term *caeruleum* is a generic term for blue pigments, equivalent to the Greek *kyanos*, and Pliny uses it interchangeably to describe Egyptian, Scythian, Cyprian blues, and blue pigments from Spain and Puteoli (Plin. *HN* 33.161) [56]. *Indicum,* as its name suggests, is an imported material corresponding to the dye known as indigo blue and can, therefore, not be related to an inorganic artificially produced blue. *Lomentum*, on the other hand, is produced, according to Pliny, by washing and grinding *caeruleum*. Unfortunately, Pliny does not specify the type of blue pigment used for its production. He does, however, inform us that *lomentum* is not suitable for use with lime and should rather be used on clay surfaces, pointing to finely ground azurite $Cu_3(CO_3)_2(OH)_2$, since azurite turns into green copper salts in basic environments [1,4]. *Caeruleum Vestorianum*, the most expensive among the blue pigments, is

produced according to Pliny by the finest quality of Egyptian blue. Its name indicates that it is made in Vestorius's workshop, which was established in Puteoli during the first century BCE, according to Vitruvius's famous excerpt on Egyptian blue (Vitr. *De arch*. 7.11) [57]. The fact that according to Pliny *caeruleum Puteolanum* or *Vestorianum* can be used close to windows [56], reinforces the hypothesis that it is, indeed Egyptian blue, since it illustrates the material's stability in outdoor conditions and in direct exposure to light.

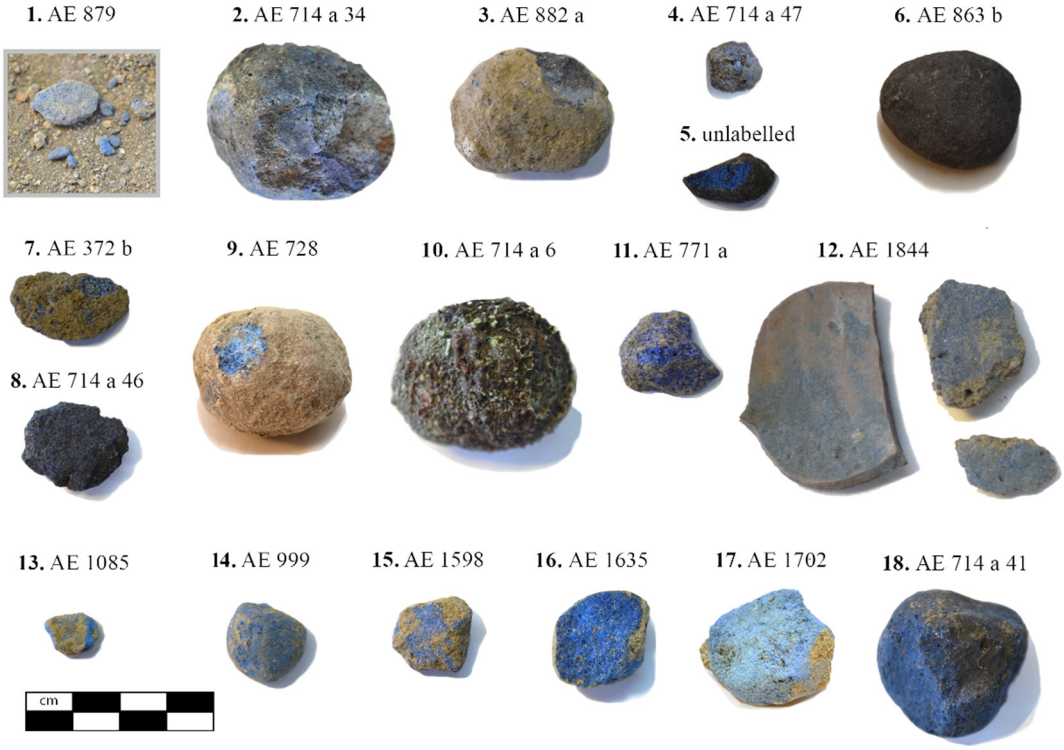

Figure 2. The Egyptian blue finds from the Koan workshop analysed in the present article.

Based on textual evidence alone, conclusions about the technology of Egyptian blue production and the different qualities of blue pigments are not straightforward. Archaeological research however often unearths the material remains of production, such as the evidence from the workshop on Kos. The study of such remains, combined with the scientific examination of archaeological finds, can deepen our understanding of past technological processes.

This paper aims to investigate the technological processes involved in the production of blue pigments in the Koan workshop and identify the possible variations employed for the production of blue pigments of lighter tones. For this purpose, eighteen representative samples were obtained from pellets of varying tones and textures of blue and prepared in cross-sections. The samples were examined through optical and scanning electron microscopy, coupled with energy-dispersive X-ray spectroscopy (SEM-EDS) and micro-Raman spectroscopy. The combination of optical microscopy, SEM-EDS, and micro-Raman spectroscopy allows the comprehensive chemical and mineralogical characterisation of the grains that compose the finds, which can inform us of the use of raw materials, the firing conditions, and the secondary processing of pellets for the manufacture of various shades of blue. The results illustrate the sophisticated technological processes employed by the craftspeople on Kos in the first century BCE.

Table 1. Description of sampled finds (EB = Egyptian blue, FS = fire structure as indicated in Figure 1).

Sample	Find	Location	Description of Find
1	AE 879	W of FS2/NE of FS3	EB fragments observed among a soil sample.
2	AE 714 a 34	FS1	EB fractured pellet, with limited brown areas.
3	AE 882 a	NW of FS3	EB fractured pellet, light blue to grey.
4	AE 714 a 47	FS1	Fragment from EB pellet.
5	unlabelled	unknown	Fragment from EB pellet.
6	AE 863 b	FS1	EB pellet of dark-blue tone.
7	AE 372 b	south room	Fragment from EB pellet; very coarse blue and green grains, loosely connected agglomerates.
8	AE 714 a 46	FS1	Fragment from EB pellet of dark blue tone; very coarse, loosely connected agglomerates with brown encrustations.
9	AE 728	Wall 4	Fractured EB pellet.
10	AE 714 a 6	FS1	Unsuccessfully produced EB pellet; grey-green surface with red metallic granules adhered.
11	AE 771 a	south room	Fragment from EB pellet.
12	AE 1844	Stoa, W of workshop	Fine-grained EB material mixed with soil, found attached on a pottery sherd.
13	AE 1085	E of workshop	Light blue, fine-grained lump with high tinting power.
14	AE 999	sporadic find	Fractured EB pellet.
15	AE 1598	EW street, E of workshop	Fractured EB pellet.
16	AE 1635	E of workshop	Fractured EB pellet.
17	AE 1702	E of south room	Fractured light blue, fine-grained pellet.
18	AE 714 a 41	FS1	Fractured EB pellet.

2. Materials and Methods

2.1. Sampling and Sample Preparation

Samples were collected from seventeen Egyptian blue pellets of varying shades and textures, including saturated blue pellets, one unsuccessfully produced pellet, as well as pellets of darker and lighter blue tones. Moreover, one sample was obtained from a finely ground powder adhered on a pottery sherd (Figure 2, Table 1). Sampling was limited to the already fractured Egyptian blue pellets. The eighteen samples were embedded in a methacrylate-based light-curing resin (Technovit 2000 LC, Kulzer, Wehrheim, Germany) using EasySections (precast Perspex sample containers by VWFecit, London, UK). The sample preparation process was carried out under a stereomicroscope (LEICA MZ6, Leica Microsystems, Wetzlar, Germany). The specimen was carefully placed with tweezers on a bed of resin in the specimen well. The samples were oriented using a tungsten needle, and the light-curing resin was placed by a disposable pipette. The prepared cross-sections were cured under blue light for 5 min in the Technotray light polymerisation unit (Kulzer GmbH, Wehrheim, Germany). The "Technovit 2000 LC" covering varnish was applied, and the cast samples were left overnight. The surface of the specimens was revealed by polishing using a series of Micromesh polishing sheets of increasing grit size from 1500 to 12,000 mesh/in.

2.2. Optical Microscopy

The cross-sections were observed with a Leica DM2700P microsystem (Leica Microsystems, Wetzlar, Germany), equipped with Leica N PLAN EPI objectives (5×/0.12 POL, 10×/0.25 POL, 20×/0.40 POL, 40×/0.65 POL, 100×/0.85 POL). The oculars magnification is 10×, while the camera mount has a 0.55× magnification. The camera is a Leica MC190 HD (Leica Microsystems, Wetzlar, Germany). The incident light is produced by a LED lamp (LH113) for the illumination of the samples. The micrographs were taken in bright field

(BF) and under polarised light in reflectance mode. The microscope was operated using the LAS X software (Leica Microsystems, Wetzlar, Germany).

2.3. Scanning Electron Microscopy Energy-Dispersive X-ray Spectroscopy

A FEI Quanta 450 Scanning Electron Microscope (FEI-Thermo Fisher Scientific, OR, USA) was used for the analysis of the cross-sections. The microscope is coupled with an Oxford X-Max^N 50 mm^2 SSD detector, which, for maintenance reasons, was replaced with an Oxford X-Max^N 20 mm^2 SSD detector (Oxford Instruments, Oxford, UK) for the analysis of Samples 10 and 16. The measurements were performed using 20 kV accelerating voltage without a conductive coating of the samples, allowing their further study with Raman microscopy. Surface charging was avoided by using the low vacuum mode (30 Pa). The instrument was operated using the Aztec 3.1 SP1 software by Oxford Instruments (Oxford, UK). The spot size was set to 5.5. The working distance used for the EDS analysis was 10 mm.

The backscattered electron (BSE) micrographs were analysed and processed with the Fiji (Image J) software [58,59]. The maximum dimension of a number of cuprorivaite and quartz particles, for which the edges could be clearly observed, were measured for each sample using the measuring tool of Fiji (Table A1). Moreover, Fiji was used for the semiquantitative presentation of the different phases, based on the various levels of grey observed in the BSE micrograph, which correspond to different elemental compositions. For this purpose, the raw .tiff BSE micrographs were first transformed into 8-bit images and analysed using the threshold tool of Fiji. The qualitative characterisation of the roundness of the particles is based on Adams [60], and the qualitative descriptions of the sizes follow the definitions by Feller and Bayard [61].

2.4. Micro-Raman Spectroscopy

Raman spectra of the eighteen cross-sectioned samples were recorded using a confocal inVia Reflex Raman microscope (Renishaw, Wotton-under-Edge, UK) equipped with a grating of 2400 mm^{-1} (vis) and a 1040 × 256 pixels RenCam CCD detector. The measurements were generated by the WiRE 4.2 spectral acquisition wizard. The analysis was carried out using the 514 nm laser probe with an edge filter in a spectral range from 86 to 1447 cm^{-1}. Several measurements per spot of interest were taken by increasing magnification (5×, 20×, 50×, 100×). Extended scans were also recorded for several substances, including cuprorivaite (514 nm laser probe, 102 to 3203 cm^{-1} spectral range). The slit opening was set to 65 μm. Laser power (0.05% to 100%), exposure time (1 to 25 s), and the number of accumulations (1 to 100) were modified depending on the sample and the analysed particle. For Sample 10, additional measurements were carried out with the 785 nm edge laser probe with a grating of 1200 mm^{-1} (laser power: 0.05%, spectral range: 86 to 1447 cm^{-1}). All measurements were performed at room temperature. The Raman spectra were compared with spectra from the RRUFF™ database [62](RRUFF Project, Arizona, USA) or previously published results, specified in the following section. Finally, the Raman spectra were plotted using OriginPro (Academic 2017, OriginLab Corporation, MA, USA).

3. Results and Discussion

This section presents an overview and discussion of the results obtained from the analysis of the eighteen Egyptian blue samples, starting from general overarching observations of the successfully produced pellets and moving to detailed descriptions of the most characteristic examples of samples of darker and lighter tones and the discussion of the results from the unsuccessfully produced pellet.

Under the optical microscope, all samples (except Sample 10, obtained from the surface of an unsuccessfully produced pellet, discussed below) present a saturated blue colour due to the presence of euhedral blue crystals (Figures 3 and A1). The study of both optical micrographs and BSE micrographs

permits the localised EDS analysis of single grains and the comparison of the elemental composition to the colour of the grain. The elemental composition of the blue grains is in agreement with the stoichiometry of the copper-calcium-tetrasilicate crystal ($CaCuSi_4O_{10}$), equivalent to the naturally occurring mineral cuprorivaite [52,53]. Under the microscope, the cuprorivaite crystals are euhedral with a platy habit parallel to 001, in accordance with the idealised morphology of cuprorivaite [52], often featuring a striated surface.

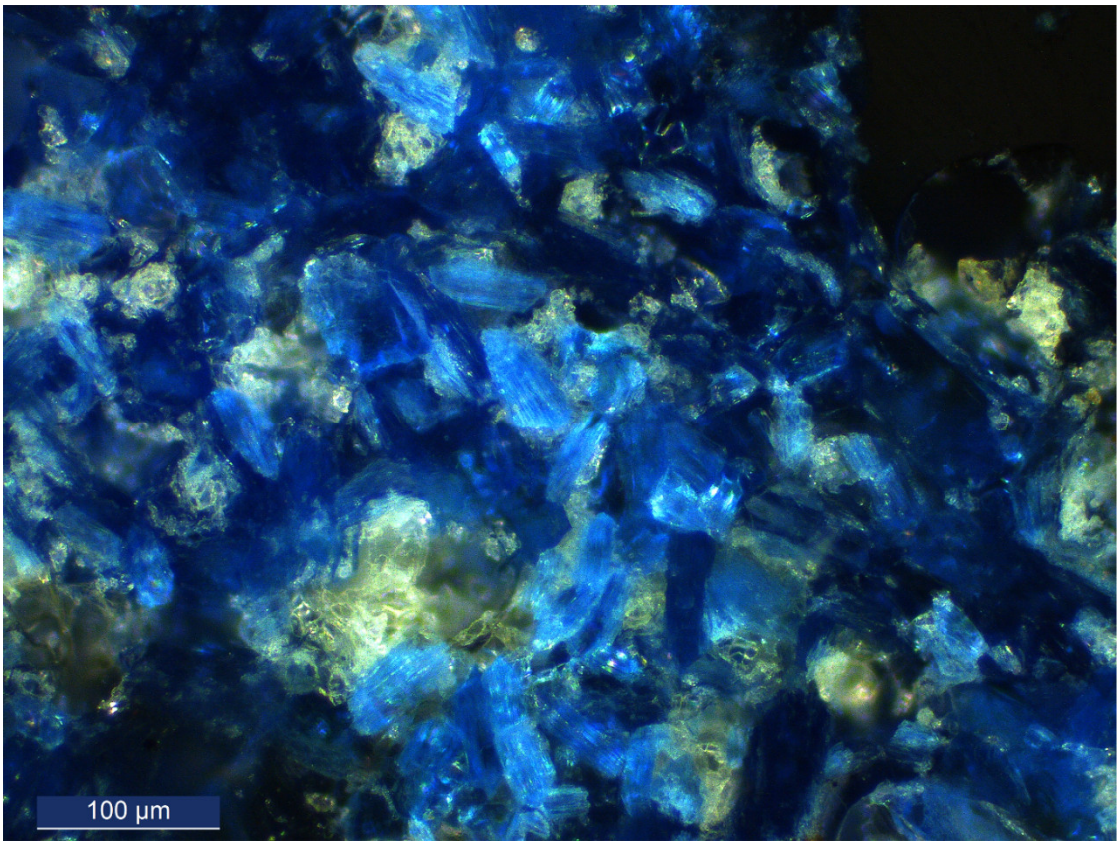

Figure 3. Optical micrograph of cuprorivaite crystals (cross-section of Sample 15, magnification 150×) in crossed polarised light.

The micro-Raman spectra of the blue crystals have the characteristic pattern of cuprorivaite, with Raman shifts approximately at 113 (s), 138 (s), 163 (vw), 186 (vw), 196 (w), 215 (vw), 231 (vw), 247 (vw), 360 (s), 378 (s), 430 (vs), 475 (w), 570 (w), 595 (w), 613 (vw), 762 (w), 776 (vw), 788 (w), 967 (w), 990 (w), 1014 (w), 1084 (s), 1103 (w), and 1143 (w) cm^{-1} (Figure 4). The strong (s) and very strong (vs) Raman shifts observed in the spectra are in agreement with previous applications of Raman spectroscopy on Egyptian blue [3,16,43,44,63–65]. The localised, single-grain Raman spectra obtained through the present research provide the complete spectrum of cuprorivaite, including weak (w) and very weak (vw) contributions. The observed variation in the Raman spectra of the different cuprorivaite crystals (Figure 4) can be explained by the polarisation effect, which is dependent on the orientation of the crystals in the embedded samples [44]. The very weak peak at 460 cm^{-1} observed in some of the cuprorivaite spectra is attributed to quartz.

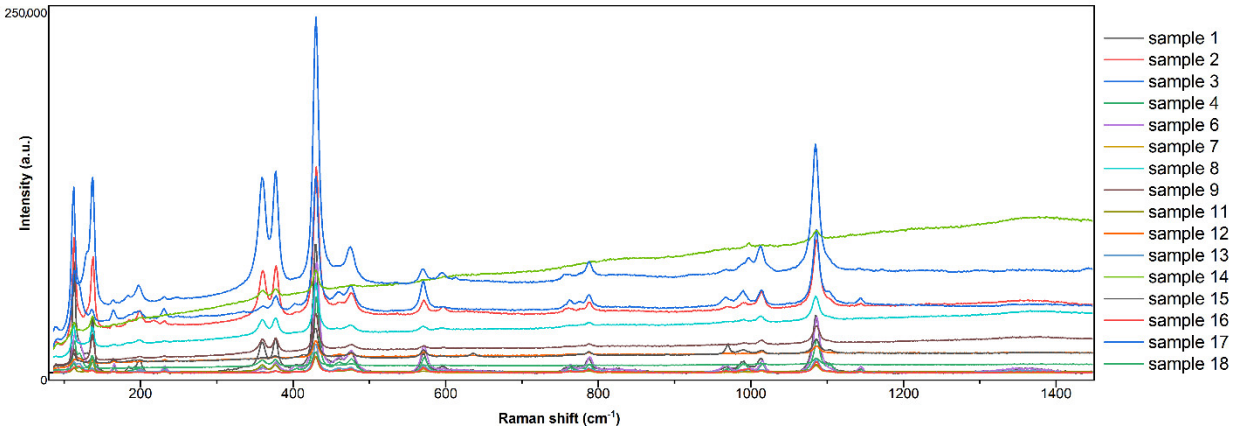

Figure 4. Raman spectra of single EB crystals detected in the different samples. The variations in the intensity of the different peaks across the different crystals, illustrates the polarisation effect observed due to the different orientation of the crystals in the cross-sections, as observed by Pagès-Camagna et al. [44]. The characteristic Raman shifts of cuprorivaite were observed at: 113 (s), 138 (s), 163 (vw), 186 (vw), 196 (w), 215 (vw), 231 (vw), 247 (vw), 359 (s), 378 (s), 430 (vs), 475 (w), 570 (w), 595 (w), 613 (vw), 762 (w), 776 (vw), 788 (w), 967 (w), 990 (w), 1014 (w), 1084 (s), 1103 (w), and 1143 (w) cm^{-1}.

SEM-EDS and micro-Raman spectroscopy confirmed the presence of quartz grains (SiO_2) in the studied samples (Figure 5). Moreover, amorphous silica exhibiting Raman bands at 599, 812, and 998 cm^{-1} was identified in Sample 6 (Figure 5).

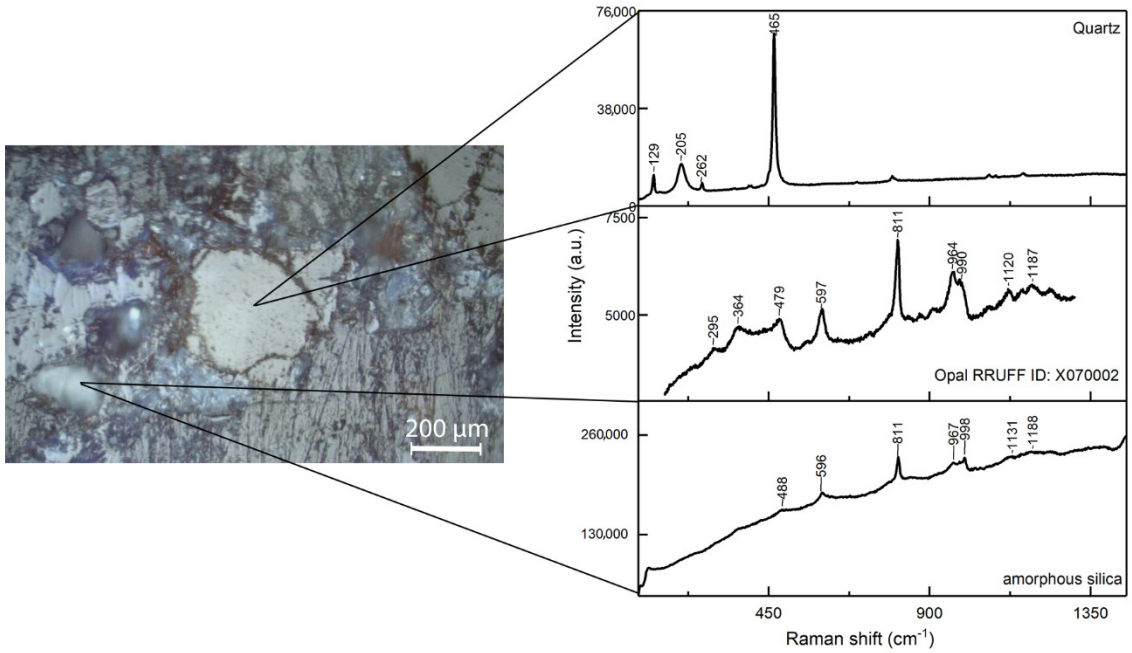

Figure 5. Raman spectra of quartz and amorphous silica detected in Sample 6.

The analysis showed the limited presence of an amorphous glassy phase among some of the studied samples (Figures 6 and 9). Such glassy phases are expected to be formed during the firing of quartz in high temperatures in the presence of alkali fluxes. In the studied samples, however, we observe that the glassy

phase is not extensively formed; rather, it is limited to the borders of the quartz grains (Figure 6c) and rarely preserved between the clusters of cuprorivaite crystals (Figure 7a). Moreover, the elemental composition of the glassy phase is not homogeneous and varies throughout the samples. Sodium, up to 5% weight, is found in the glassy phases through the localised EDS analysis, along with potassium in lower concentrations (Table 2, Figure 7b). Phosphorus was also detected in most samples (Table 2). According to Jaksch et al. [41], the presence of phosphorus is indicative of a plant source for the alkali flux.

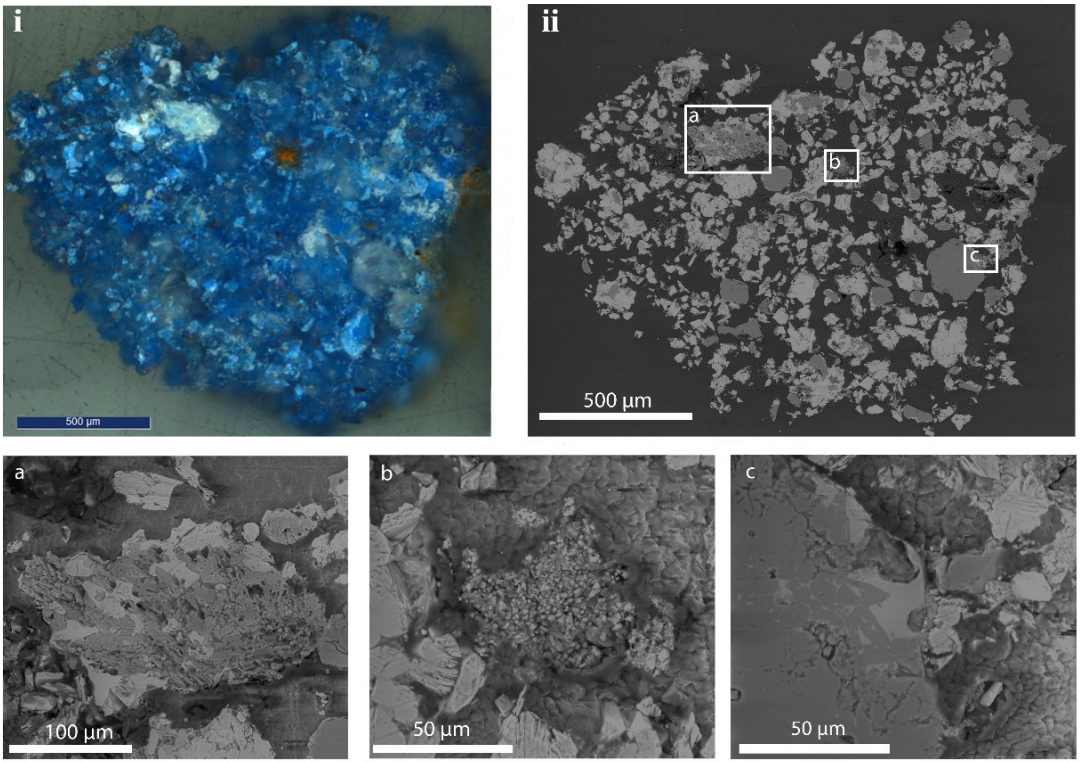

Figure 6. (**i**) Optical and (**ii**) BSE micrograph from Sample 1. (**a**–**c**) BSE micrographs of higher magnification were obtained from different areas of interest (marked here as (**a**–**c**) in (**ii**)). The different shades of grey in the lower three BSE images represent variations in the elemental composition of the particles: brighter particles correspond to cuprorivaite crystals and agglomerates, dark grey particles are quartz, and the grey in between indicates the glassy phase. The BSE micrograph of area (**b**) corresponds to the red dot observed in the optical micrograph, which was identified as an iron-rich impurity.

While it is possible that the glassy phase is lost due to weathering, thus biasing our interpretations, as Hatton et al. suggest [48], the study of the preserved glassy phases can reveal important details about the production process. Experimental reconstructions have shown that during the firing of the starting materials, the quantity of the alkali flux used is crucial for the formation of the glassy phase and governs the mechanism of the cuprorivaite synthesis [49]. A starting mixture with a high alkali content leads to the dissolution of the quartz grains and to the formation of an extended glassy phase in the final product where the copper and calcium ions are dissolved and in which the cuprorivaite crystals are formed [49]. However, if the alkali content is insufficient (<2%), the glassy phase cannot be extensively formed, and the cuprorivaite crystal formation is carried out in a solid-phase reaction through the diffusion of ions in the borders of the quartz grains [49]. The latter eventually results in a more heterogeneous material [49]. The restricted presence of glassy phases observed in the studied samples from the Koan workshop suggest the limited use of alkali fluxes in the production process [27,49]. The absence of an extended glassy network throughout the matrix of the material would prevent the diffusion of ions in the melt and, therefore, result

in the heterogeneity of the limited glassy phases formed. Moreover, limited control over starting materials and poor mixing and grinding prior to firing may have caused this variation.

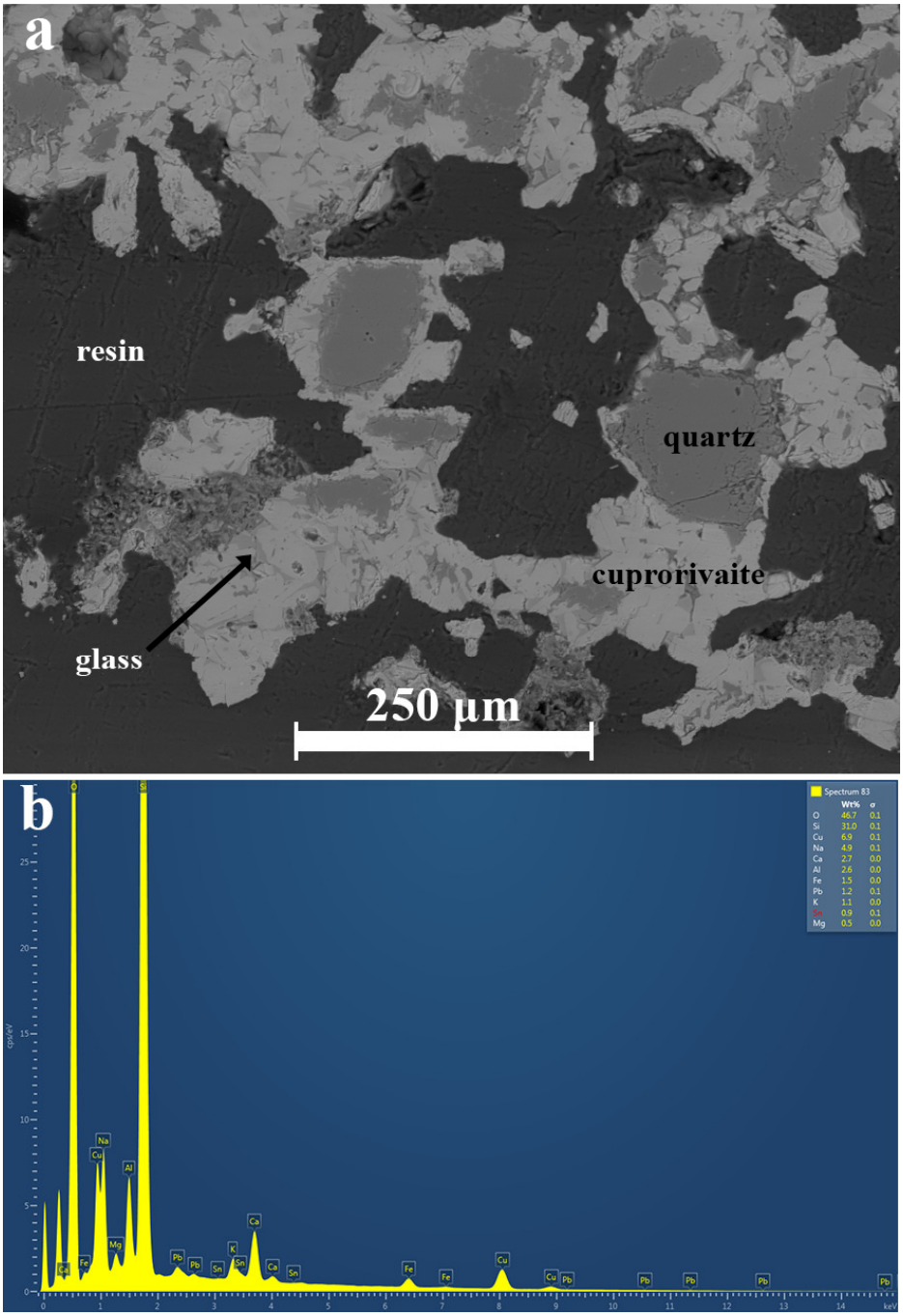

Figure 7. (**a**) Detail from the BSE micrograph of Sample 5. The cuprorivaite particles (light grey) form clusters surrounding the partially dissolved quartz grains (dark grey). A limited glassy phase (mid grey) is preserved in between the cuprorivaite particles. (**b**) EDS spectrum of the Cu-rich glassy phase present in Sample 5 with a high Na content.

Table 2. Summary of the results from the EDS and micro Raman spectroscopy per sample.

Sample	EDS			Raman Spectroscopy
	Major	Minor	Trace	
1	O, C, Si, Cu, Ca	Fe	Pb, S, Al, Mg, K, Na, Sn, Au	Cuprorivaite, quartz
2	O, C, Si, Cu, Ca	Fe, Al	S, Na, As, P, Cl, Pb, Mg, Al, Sn, K, Ti	Cuprorivaite, quartz, calcite
3	O, C, Si, Cu, Ca	Fe	Al, Pb, S, Mg, Na, Sn, Au, As, P, K, Na, Ti, Cl	Cuprorivaite, quartz, tenorite
4	O, C, Si, Cu, Ca	Fe, Al	P, K, Na, Fe, Mg, Pb, Sn, Na, Cl	Cuprorivaite, quartz, calcite
5	O, C, Si, Cu, Ca	Fe, Al	Pb, Sn, K, Mg, Na, S	Cuprorivaite, quartz, calcite
6	O, C, Si, Cu, Ca	Fe, Al, Na	Sn, Mg, Pb, K, P, Na, S, Ti, Cl	Cuprorivaite, quartz, amorphous silica
7	O, C, Si, Cu, Ca	Fe, Al	Mg, K, S, Na, P, Ti, Sn, Pb	Cuprorivaite, quartz, calcite, anatase
8	O, C, Si, Cu, Ca	Fe, Al, Pb	K, Na, Mg, Cl, S, P, Na, Sn, Au	Cuprorivaite, quartz, graphite, crystalline silicon
9	O, C, Si, Cu, Ca	Fe, Al, Pb, Na	Cl, Na, Pb, K, Sn, Mg, Ti, P	Cuprorivaite, quartz, tenorite
10	O, C, Si, Cu, Ca	Fe, Al, Pb	Mg, K, Cl, P, Sn, Ti	Quartz, chrysocolla
11	O, C, Si, Cu, Ca	Sn	Pb, Fe, Na, Al, P, Mg, Cl, K, Ti	Cuprorivaite, quartz, malayaite
12	O, C, Si, Cu, Ca	Al, Mg, Cl, Na, K, Fe, Pb	P, Mn, Na, Sn, Ti	Cuprorivaite, quartz, amorphous carbon, magnetite
13	O, C, Si, Cu, Ca	Fe, Co	Ni, Sn, Mg, Na, Al, K, Zn, Pb, Cr, S	Cuprorivaite, quartz, rutile, anatase, $CoFe_2O_4$ particles
14	O, C, Si, Cu, Ca	Sn, Al, Na	Fe, K, Pb, Cl, Mg	Cuprorivaite, quartz
15	O, C, Si, Cu, Ca	Sn	Na, Fe, Al, P, Mg, Cl, K, Ti	Cuprorivaite
16	O, C, Si, Cu, Ca	Sn	K, Sn, Na, Cl, Al, Zr, S, Pb, P	Cuprorivaite, quartz, anatase, amorphous carbon
17	O, C, Si, Cu, Ca	Sn	Al, Fe, Na, K, Zr, Mo, P, Ti, S, Mn, Ni	Cuprorivaite, quartz
18	O, C, Si, Cu, Ca	Sn	Al, Fe, K, Na, Mg, Pb, S, Cl, Ti, P	Cuprorivaite, quartz

In order to illustrate the main phases present in each sample, namely cuprorivaite, quartz, and glass, the BSE micrographs (Figure A2) were processed with the Fiji (Image J) software. The different levels of grey observed in the BSE micrographs correspond to different elemental compositions, since heavy elements appear brighter than lighter ones (Figure 8). Based on the variation of the contrast of the BSE micrographs, the concentration of the cuprorivaite, quartz, and glassy phases could be semiquantitatively estimated (Figure 9, Table A2).

Moreover, the variation in the size and shape of the quartz grains and the cuprorivaite particles may shed light on the production process, the selection of raw materials, and the colour of the final product. Therefore, the morphology of the quartz and cuprorivaite grains was examined (Table 3). Finally, the

maximum and minimum size of the quartz and cuprorivaite particles, as well as of the cuprorivaite agglomerates were measured using the Fiji (Image J) software for each sample (Figure 10, Table A1).

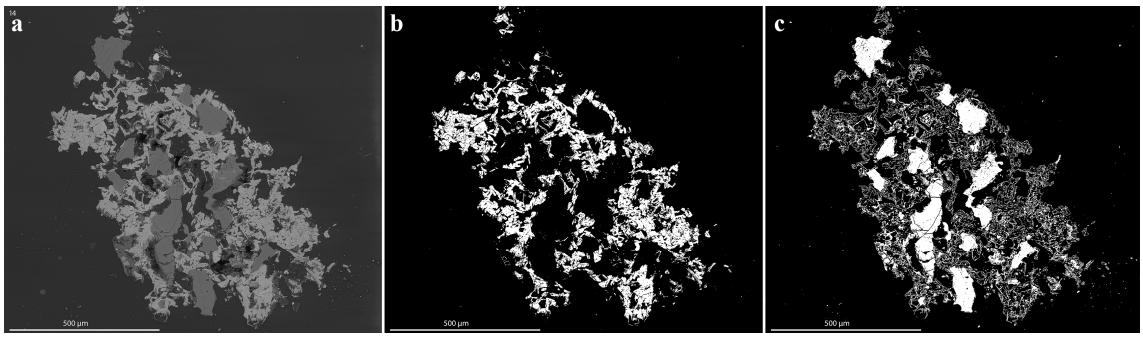

Figure 8. (**a**) BSE micrograph of Sample 14. The brighter euhedral grey particles represent cuprorivaite, and the darker grey anhedral and subangular particles belong to quartz. The processed micrographs (**b**,**c**) depict isolated particles of (**b**) cuprorivaite and (**c**) quartz particles, demonstrating the bimodal distribution of the particle size and better illustrating the grain morphology. The processed micrographs were used for the qualitative assessment of the different phases (see Figure 9).

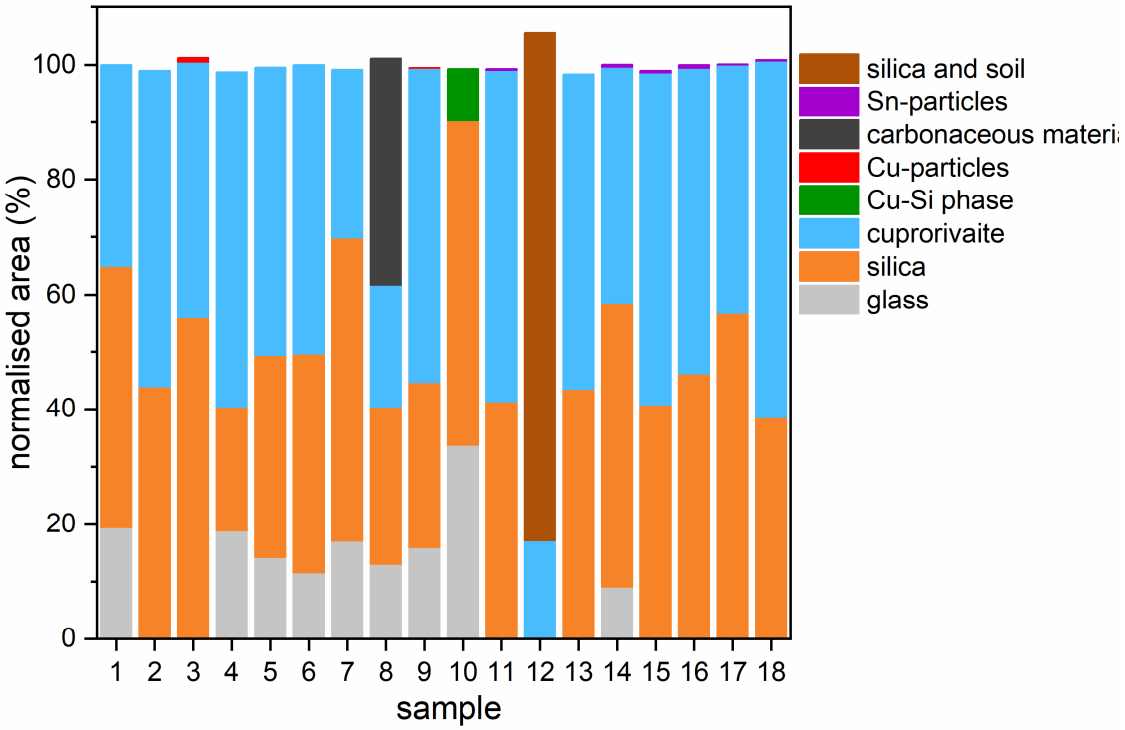

Figure 9. Area (%) of the various phases present in the analysed samples. The area (%) calculations are based on the image analysis of the BSE micrographs using the Fiji (ImageJ) software (see also Table A2). The areas are normalised to the total area without the resin, and the graph is plotted using Origin (Academic 2017).

From the qualitative phase analysis of the BSE micrographs, we observe that quartz, as indicated by the Raman spectra, is present in all samples (Table 2, Table A2). Quartz is the only starting material that does not entirely melt in the high temperatures required for the production of Egyptian blue (850–1050 °C), without the presence of a sufficient quantity of an alkali flux. Therefore, the morphology of the quartz

grains may hold information about the choice of raw materials for the silica source. According to Vitruvius (*De arch*. 7.11) [57], sand was used for the production of Egyptian blue in the first century BCE workshop of Vestorius in Puteoli. Indeed, the use of quartz sand has been supported in previous studies on Egyptian blue based on the presence of titanium and iron impurities as well as the rounded shape of the quartz particles [41,46,48]. The rounded shape of the quartz particles in the Koan samples analysed here (Table 3) as well as the presence of titanium and iron impurities (Table 2) suggest the use of sand for the production at the Koan workshop.

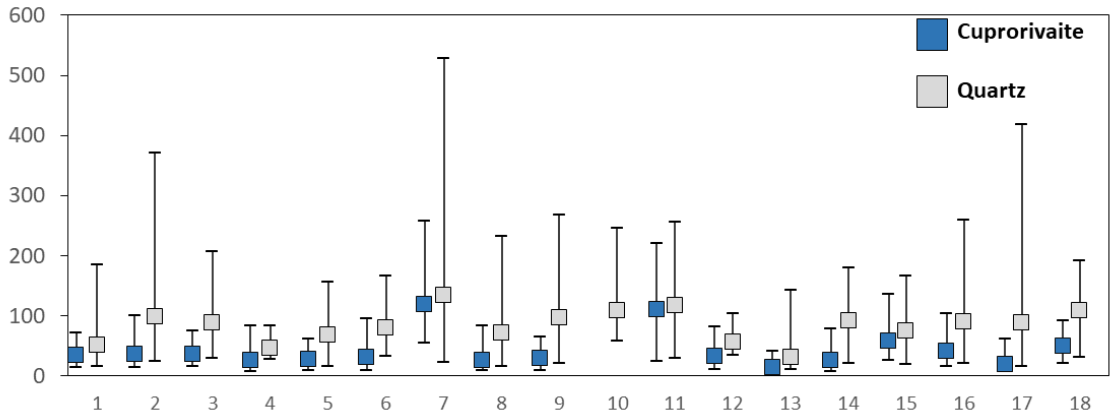

Figure 10. Average, maximum, and minimum particle sizes for cuprorivaite (blue) and quartz (grey). The average size of the particles is based on a number of measurements of single grains with distinguishable edges, observed in the BSE micrographs (Table A1).

Table 3. Quartz and cuprorivaite particle morphology based on the BSE micrographs.

Sample	Quartz	Cuprorivaite
1	High sphericity angular	Euhedral and subhedral, striated platy particles
2	Low sphericity subangular	Subhedral, striated and cleaved platy particles
3	High sphericity subangular to rounded	Subhedral, striated and cleaved platy particles
4	Low sphericity subangular to rounded	Euhedral platy particles
5	High sphericity rounded, subangular	Euhedral platy particles
6	Midsphericity subrounded	Euhedral platy particles
7	Subrounded elongated	Subhedral, striated and cleaved particles
8	Rounded to subangular high sphericity	Euhedral platy particles, cleaved
9	Angular to subangular low to medium sphericity	Euhedral platy particles
10	Subrounded high sphericity	No cuprorivaite particles observable
11	Rounded high sphericity	Euhedral platy particles
12	Rounded high sphericity	Euhedral and cleaved particles
13	Angular mid sphericity	Subhedral to anhedral particles
14	Subangular low to high sphericity	Euhedral platy particles
15	Subangular to angular high to low sphericity	Euhedral platy particles
16	Angular to subangular high to low sphericity	Euhedral platy particles
17	Angular to subangular mid sphericity	Euhedral, cleaved particles
18	Angular to subrounded mid to high sphericity	Euhedral platy particles

The partially dissolved borders of the quartz grains due to the attack of the alkali fluxes and the local formation of a glassy phase (see for example the detail in Figure 6c), complicates the characterisation of the original grain morphology. The presence of very coarse (up to 528 μm) quartz grains suggests the use of beach sand in contrast to the fine quartz particles deriving from desert sand [66,67]. However, the material from Kos shows a broad grain size distribution for the quartz particles, ranging from 10 μm to 528 μm

(Figure 10, Table A1). Moreover, the observed quartz particles are angular to subangular (Table 3). While this morphology is expected for beach sand, the angular shape of the quartz grains possibly indicates a grinding process. It is perhaps worth noting that the sand found at the Lambi beach, located in proximity to the workshop area (see map in Figure 11e, contains large quartz grains that can easily be selected and separated by hand from the rest of the grains (Figure 11), suggesting a possible local source of pure quartz. However, further research is required to test this hypothesis. As Giménez et al. demonstrated in a 2017 study, the presence of NaCl results in the formation of wollastonite and not cuprorivaite, since copper remains embedded in the amorphous phase [68]. Therefore, quartz beach sand should be washed before being used for the production of Egyptian blue to remove NaCl, which would otherwise affect the synthesis of cuprorivaite [68].

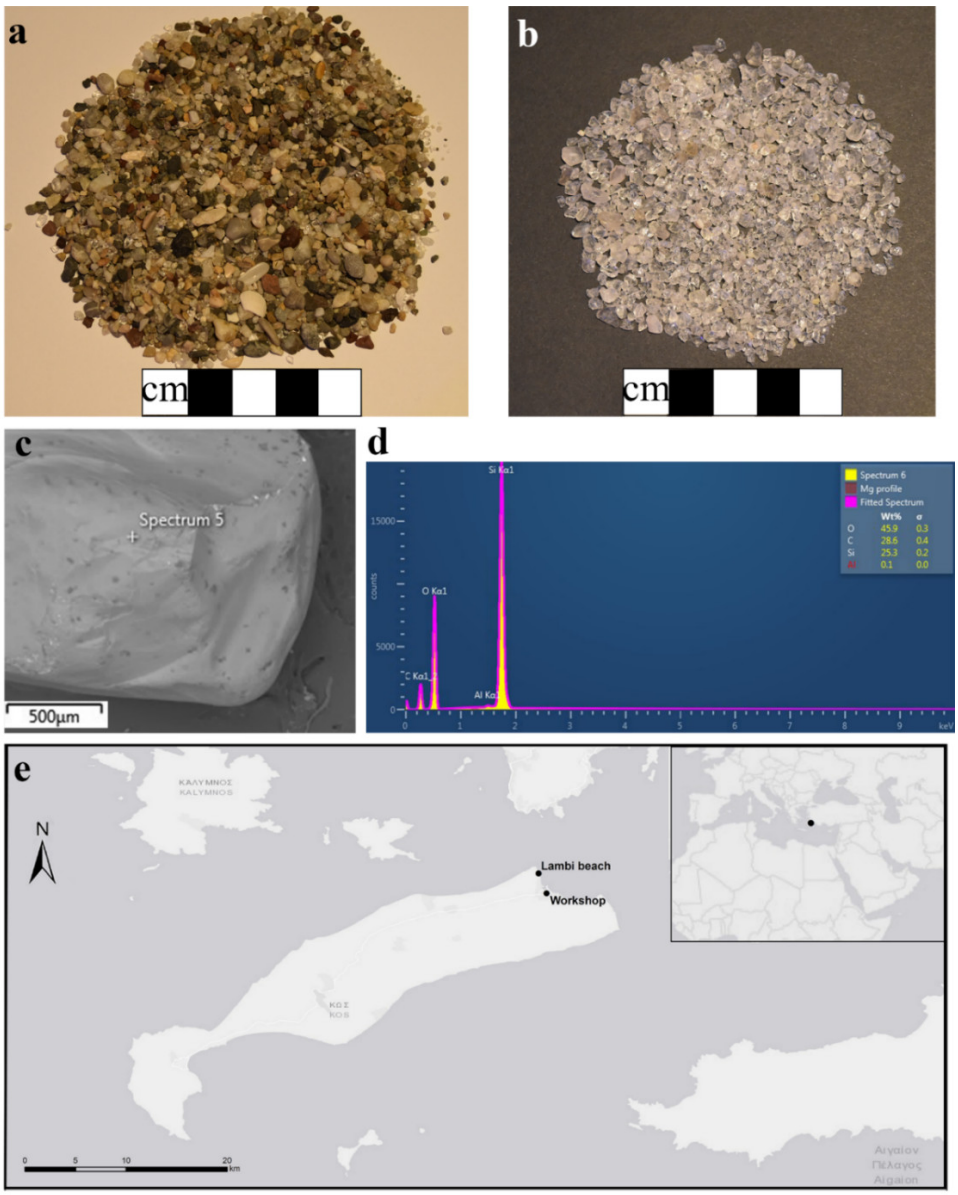

Figure 11. (**a**) Local beach sand (from Lambi beach) with large quartz grains; (**b**) quartz particles separated (hand selection) from the sand; (**c**) BSE micrograph of quartz grain; (**d**) EDS analysis of quartz grain; (**e**) map of Kos with the beach and the workshop location denoted (produced by Mncedisi Sitaleki).

The dimensions of the cuprorivaite particles, which appear brighter than the quartz grains and the glassy phases in the BSE micrographs, range from 3 to 258 μm in length (Figure 10, Table A1). In addition, the cuprorivaite particles form closely packed agglomerates, with dimensions ranging from 25 to 800 μm across (Table A1). The electron micrographs demonstrate that the cuprorivaite crystals are formed largely in contact with the quartz grains (Figure 7). This micromorphology is characteristic of the solid-state production process by the solid-state diffusion of elements at the interface with various grains, as proposed by Delamare [49] (see discussion above on the presence of the glassy phase). According to Delamare, this production process is typical for Roman Egyptian blue and indicates a limited quantity of alkali fluxing agents in the starting mixture [1].

To summarise, the so far discussed results from the analysis of the successfully produced Egyptian blue pellets, suggest the use of a washed and possibly ground quartz as a silica source, while the availability of quartz-rich sand indicates a possible local resource. Moreover, the absence of an extended glass-phase indicates a low-alkali starting mixture.

Besides copper, calcium, silicon, and oxygen, the elements that compose cuprorivaite, several other minor and trace elements that illuminate the production process and use of starting material were detected by EDS (Table 2). Tin, iron, and lead were present in all analysed samples (Table 2). These elements are considered indicative of the raw materials used to produce Egyptian blue. The limited quantities of iron in the studied samples suggest that it is an impurity, possibly entering the mixture from the type of quartz sand used in production, thus strengthening the hypothesis that beach sand was used.

The presence of small quantities of tin is considered indicative of the use of bronze as a copper source [2,17,27,44]. Based on elemental analysis, arsenical copper alloys have been identified as the copper source for Egyptian blue production in the Old Kingdom, which was replaced by bronze scrap from the second half of the second millennium BCE and until the Roman period [1,41,50]. Later Egyptian blue productions indicate the use of brass (copper–zinc alloy) for the production of Egyptian blue [69]. These observations suggest a preference for the use of copper alloys instead of metallic copper or copper ores for the production of Egyptian blue. According to Jaksch et al., when copper–tin alloy filings (bronze) were used as a copper source, copper reacted with calcium and silica to form cuprorivaite, and the remaining tin crystallised as tin oxide [41]. Hatton has demonstrated that despite the problematic limit of tin detection (>0.3%) due to spectral overlapping in EDS, the presence of tin in Egyptian blue points to the use of bronze as a copper source [70]. In certain samples (11, 14, 15, 16, 17, 18, see also Figure 9), tin-rich nodules, separated from the copper-containing phases, were distinguished (Figure 12), similarly to other studies on Egyptian blue [1,41,44,71]. The presence of these readily distinguishable tin-containing nodules only in some of the studied samples possibly indicates the use of scrap copper alloys with a higher tin-content in their original composition.

Malayaite ($CaSnO(SiO_4)$) was identified in Sample 11, with the characteristic Raman shifts at 138 (vs), 177 (vw), 325 (m), 364 (w), 512 (vw), 573 (s), and 860 (vw) cm^{-1}, in agreement with the results from the RRUFF database (RRUFFID: R061104). The shifts at 633 and 774 cm^{-1} are attributed to cassiterite (SnO_2) [72] (Figure 12b). The spectrum also features a band at 429 cm^{-1}, attributed to cuprorivaite, and a shift at 745 cm^{-1}. The latter Raman shift has also been observed by Pagès-Camagna et al., who found particles with bands at 178, 327, 575, and 748 cm^{-1} in their analyses of Egyptian green samples [44]. However, the presence of these spectral features in the Koan samples should not be confused with Egyptian green, which is the outcome of a variation of the production [46]; rather, the limited amount of green material found among the Koan finds, including pellets with both green and blue areas, suggests the unsuccessful outcome of Egyptian blue production.

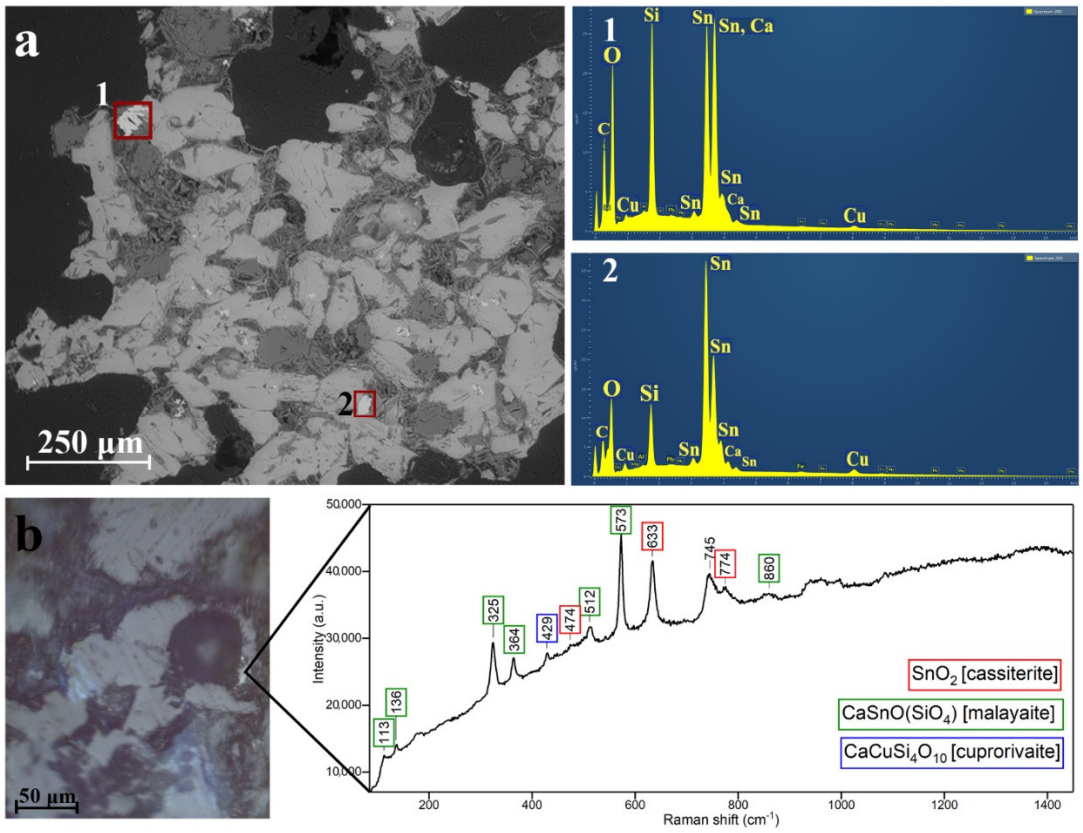

Figure 12. (**a**) Sample 11: detail of the BSE micrograph and EDS spectra from two Sn-rich areas. Area 1 corresponds to a copper–tin silicate, while Area 2 corresponds to a tin-rich phase, most likely SnO_2 (cassiterite). (**b**) Raman spectrum of Sn-rich particles with bands characteristic of $CaSnO(SiO_4)$ (malayaite) and SnO_2.

The presence of lead in all samples (Table 2) has been interpreted as indicative of the use of leaded bronze as a copper source [17]. However, the presence of amorphous lead lumps and litharge at the workshop [35,36] does not exclude the possibility of contamination from the environment. The presence of metal impurities in the studied samples, including gold (Table 2), illustrates the relationship between the production of Egyptian blue and metal-working at the Koan workshop space, as previously suggested by the identification of corroded silver attached to an Egyptian blue pellet from the workshop [36].

The observation of Samples 3, 4, and 6 with the light microscope allows the distinction of red, rounded anhedral particles, which form agglomerates (3 to 30 µm across) (Figure 13a). SEM-EDS analysis indicates that these particles are rich in copper (see, for example, Sample 3 in Figure 13b,c).

Copper (II) oxide (tenorite) was identified by micro-Raman spectroscopy on the borders of the red particles of Sample 3, with the characteristic bands at 299, 345, and 631 cm^{-1} (Figure 13d). The presence of tenorite has previously been interpreted as proof of an oxidising atmosphere during firing [44]. Tenorite, however, was limited in the studied samples, while the extensive presence of "Raman-silent" copper-containing red granules (Figure 13a,c), indicate the presence of unreacted metallic copper. This metallic copper-excess, combined with the presence of tenorite, may possibly suggest insufficient oxygen in the chamber during firing. The unreacted copper-containing particles could be responsible for the darker tones of these samples.

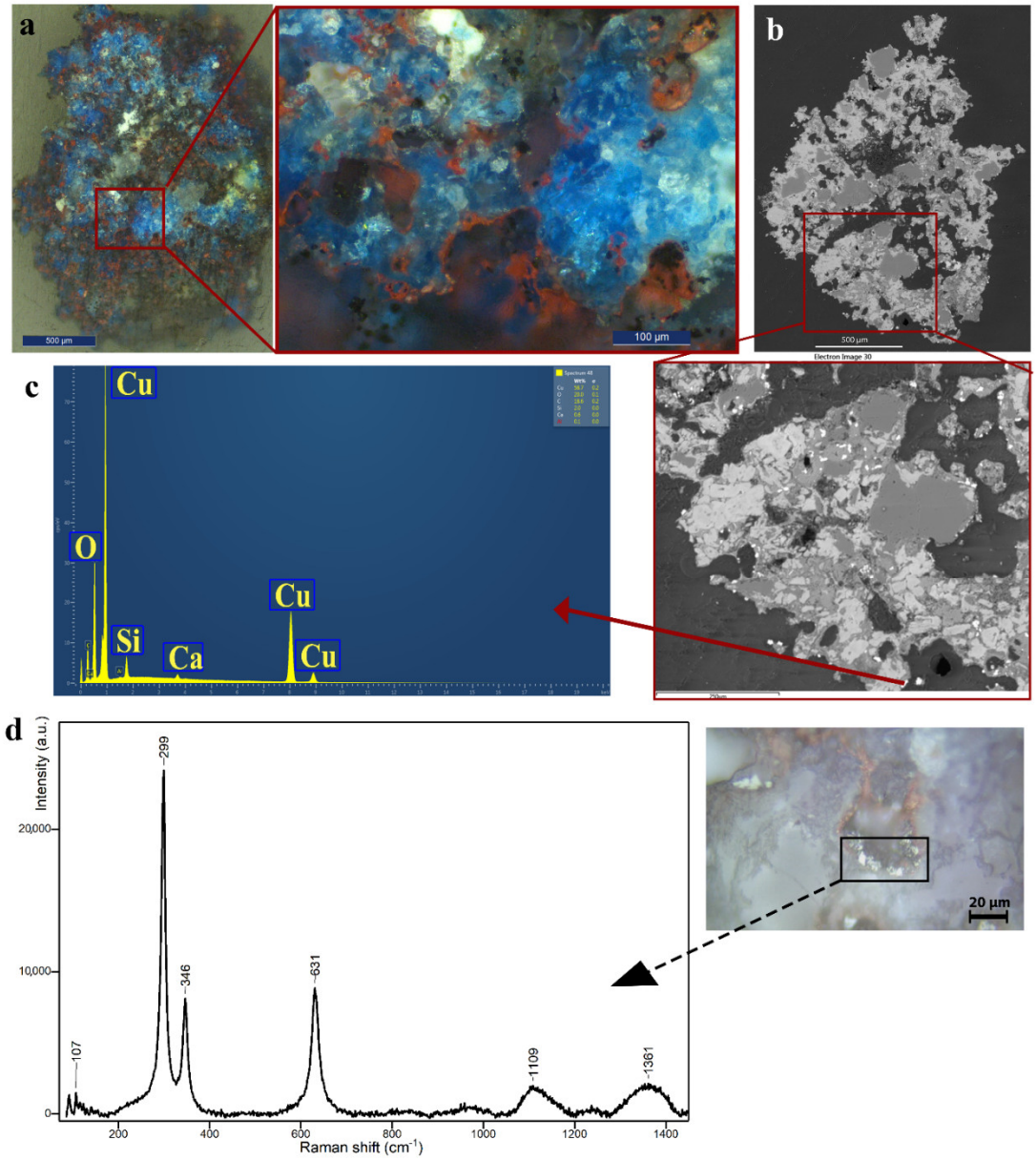

Figure 13. (**a**) Optical micrograph of Sample 3. (**b**) BSE micrograph of Sample 3. (**c**) SEM-EDS analysis of Sample 3: the EDS analysis of the bright rounded particles shows a copper-rich phase. (**d**) The borders of the red particles were identified as copper (II) oxide (CuO), with the characteristic Raman spectrum of tenorite.

The dark tone observed in the optical micrograph of Sample 8 (Figure A1) is attributed to the presence of poorly crystalline graphite, with Raman bands of graphite at approximately 1365 and 1598 cm^{-1} (Figure 14). Sample 8 was retrieved from an Egyptian blue fragment that was found in the charcoal-rich layer of the fire structure and, therefore, the presence of graphite is probably an impurity stemming from the archaeological context.

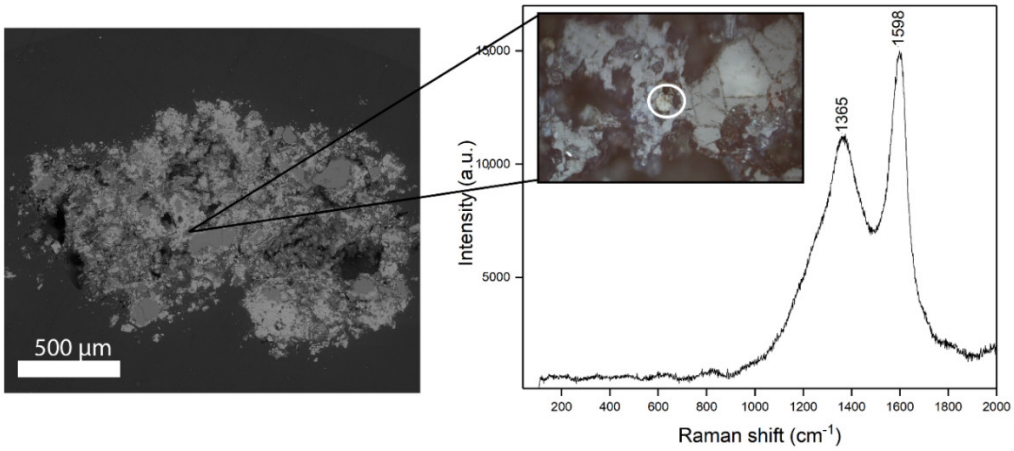

Figure 14. BSE micrograph and Raman spectrum of graphite particles observed in Sample 8.

Macroscopically, Sample 7 differs from the other successfully produced pellets, since it features a coarse texture with both blue and green grains (Figure 15a,b). The blue particles are of two types: euhedral platy particles with striated surfaces and thin, platy particles, with sizes ranging from 60 to 160 µm (Figure 15c–e). These thin particles could be the result of cleavage, suggesting the mechanical crushing of the initially formed cuprorivaite crystals. SEM-EDS and Raman analysis confirmed the identification of the blue crystals as cuprorivaite. The green colour corresponds to a Cu-Si phase, which was "Raman-silent". The coexistence of the euhedral cuprorivaite crystals with cleaved cuprorivaite particles and the amorphous Cu-Si particles could suggest a secondary treatment process, possibly related to the crushing and subsequent re-firing of the initially produced Egyptian blue pellets. It appears, however, that this secondary firing would have been abruptly interrupted before new cuprorivaite crystals were formed.

Among the analysed blue finds (Figure 2), two pellets (Samples 13 and 17) feature a lighter blue tone compared to the other successfully produced pellets. Additionally, Sample 12, deriving from loose blue grains mixed with soil, which were found attached to a pottery sherd, indicates the grinding of the initially produced blue pigment. Samples 12, 13, and 17 were characterised as Egyptian blue based on the EDS analysis and the identification of cuprorivaite through micro-Raman spectroscopy (Table 2). Besides cuprorivaite, Sample 12 contains impurities from the soil, including feldspars, as well as lead- and iron-rich particles (Table 2), most likely attributed to contaminations from the environment.

The presence of lighter blue pellets in the vicinity of the workshop suggests variations of the production process to produce different qualities of blue pigments. While it is known that the lightness of pigments increases with decreasing particle size [73], Delamare et al., in their paper on the different qualities of Egyptian blue found in Pompeii [55], conclude that the production of the lighter blue pigments is not necessarily related to the size of the cuprorivaite particles; rather, the granulometry of Pompeiian finds averaged around 100 µm for both light and dark blue. According to their results, two different production processes were employed for the production of lighter blue pigments from Egyptian blue: (a) addition of a white pigment (aragonite, cerussite, or calcite) to the initially produced material and (b) decreasing the firing time during the production process. Finally, among the lighter blue pigments studied, they identified one pellet that was composed of a copper-tinted blue glass and was, therefore, not classified as Egyptian blue [55].

Returning to the Koan workshop, the results obtained from the analysis of Samples 13 and 17 demonstrate that the lighter blue materials are composed of cuprorivaite crystals and are, therefore, variations of Egyptian blue (Table 2). The lightness in the final pigment is, however, related to the size of the cuprorivaite grains (particles or agglomerates) (Figure 10, Table A2). Indeed, the lighter blue tone of

Samples 13 and 17 (Figure 2) does not seem to be causally related to a significant variation in the elemental composition of the materials (Table 2); rather, the small size of the cuprorivaite particles, ranging from 3 to 62 μm, and the size of the cuprorivaite agglomerates, which do not exceed 130 μm (Figure 10, Table A2), appear to be responsible for these lighter tones of blue. Contrasting the observations from the Pompeian material [55], these results show a direct relationship between the particle size and the final perceived colour, with the light blue pellets being composed of smaller cuprorivaite particles (Figure 10).

The investigation of Sample 13 with micro-Raman spectroscopy revealed the presence of several dark-coloured particles (20 μm across), with the characteristic Raman shifts of partially disordered cobalt ferrite ($CoFe_2O_4$) with the structure of an inverse spinel [74,75] (Figure 16). The presence of $CoFe_2O_4$ in the Egyptian blue sample from Kos is puzzling; whether it is intentionally added to enhance the blue colour of the pigment or is present only as an impurity cannot be answered with certainty. However, the presence of several $CoFe_2O_4$ particles, combined with the small particle size of both the cuprorivaite and quartz particles and their narrow size distribution (Table A1), suggest the further treatment of the initially fired Egyptian blue pellets for the production of a fine quality of blue pigment. The analysis of the pellet indicates the crushing and grinding of the initially fired Egyptian blue, and the small size of the crystals would result in a light blue pigment [73]. Therefore, the intentional addition of cobalt-rich material would enhance the saturation of the colour.

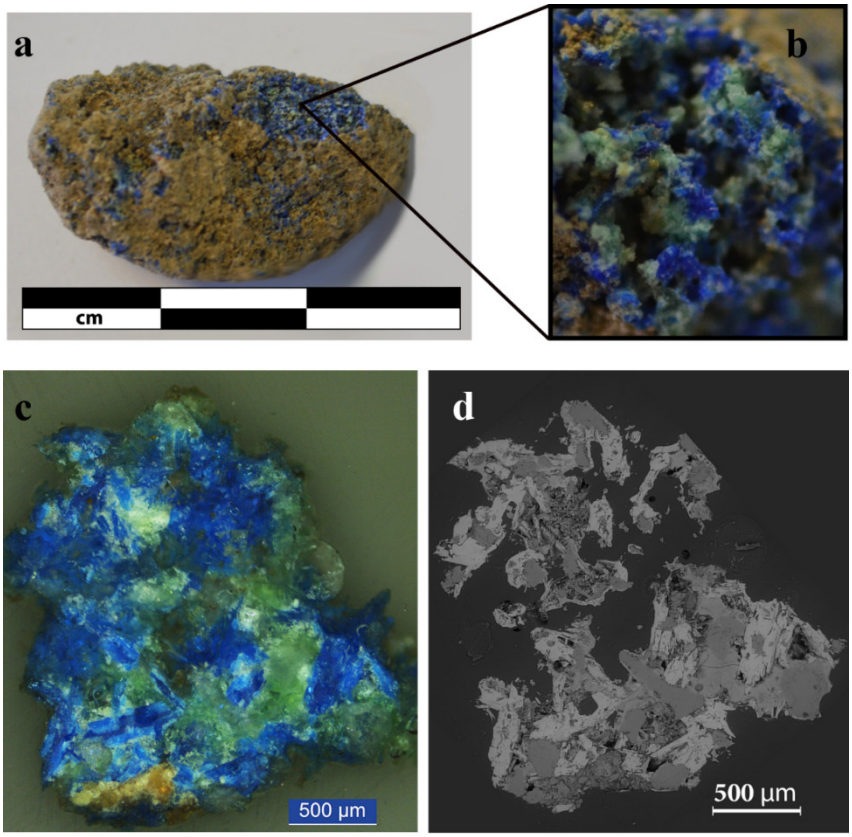

Figure 15. (**a**,**b**) The pellet from which Sample 7 was obtained features a coarse, heterogeneous matrix that consists of blue and green grains. (**c**) The optical micrograph of Sample 7 shows that two types of blue particles are present: large, euhedral cuprorivaite particles with striated surfaces and very thin, cleaved particles, possibly resulting from the crushing of larger euhedral cuprorivaite crystals. (**d**) The BSE micrograph of Sample 7 shows that the green areas correspond to quartz grains and an extended glassy phase.

The provenance of the cobalt mineral remains to be explored. It is known, however, that cobalt was used as a colouring agent for the production of blue glass and glaze in Egypt since the mid-second millennium BCE, and the source of cobalt is considered to be a type of cobaltiferous alum from the Kharga and Dakhla Oases of the Western Desert in Egypt [76]. Cobalt-based blue glazes have been identified in blue faience glazes from the coeval third century BCE to the third century CE workshop of Memphis [77], which has also been identified as an Egyptian blue production site [17,29,31].

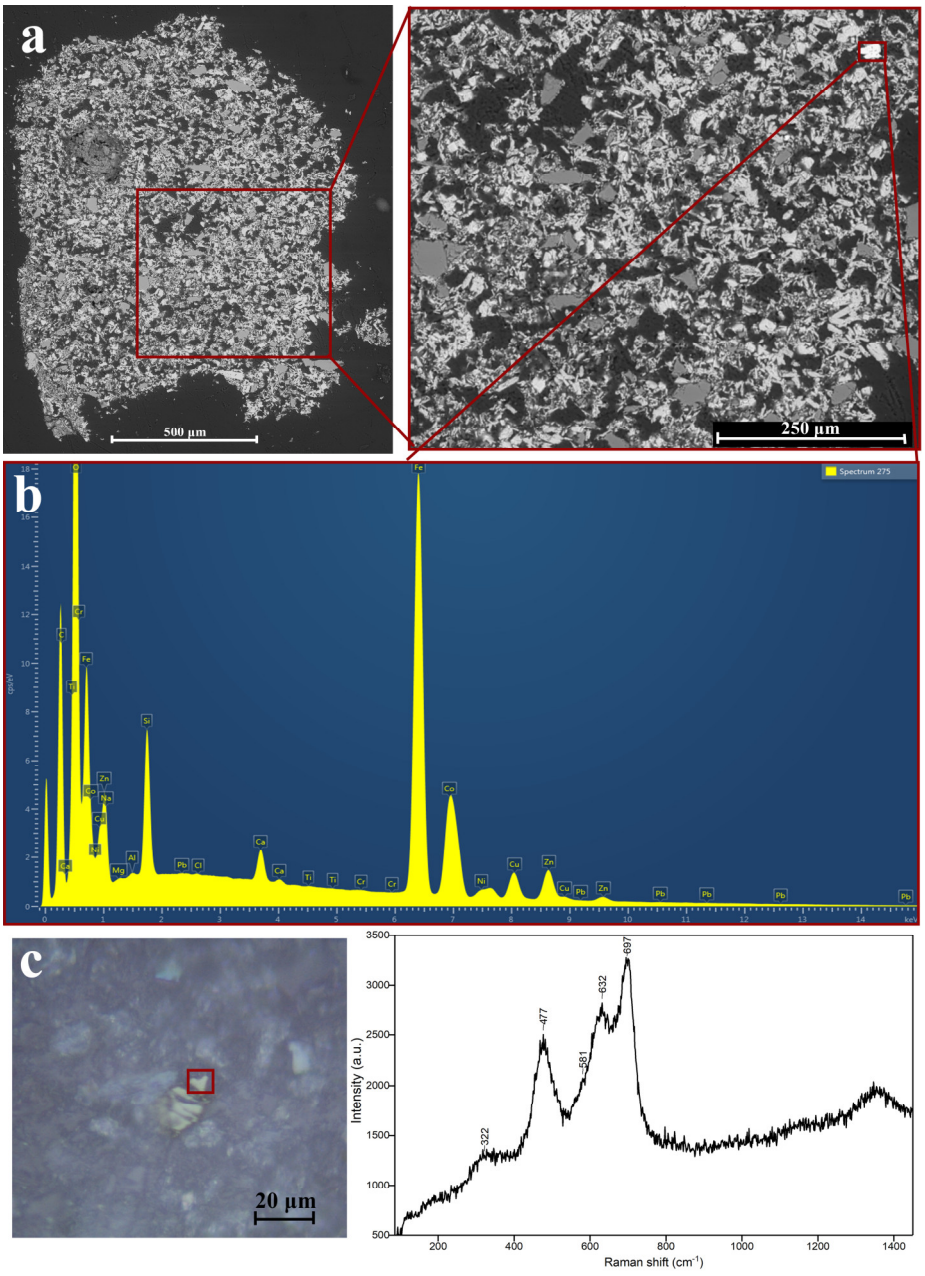

Figure 16. (**a**) BSE micrograph of Sample 13, illustrating the fine size of the cuprorivaite and quartz particles. (**b**) EDS spectrum of a bright agglomerate with high iron and cobalt content. (**c**) Raman spectrum of the particle with bands at 477, 581, 632, and 697 cm^{-1}, corresponding to partially disordered $CoFe_2O_4$ with the structure of an inverse spinel.

When observed macroscopically, Sample 17 has a less saturated colour compared to Sample 13, indicating a different production process (Figure 2). The microscopic observation of the sample revealed a significant difference between the two light blue pigments. While the size of the cuprorivaite particles does not exceed 65 μm for Sample 17, and is, therefore, comparable to Sample 13 (up to 40 μm), the size of the quartz particles is significantly larger, reaching up to 418 μm (Figures 9 and 17, Table A1). This bimodal distribution of the grain sizes indicates a variation in the technological process for the production of Sample 17. The coexistence of small cuprorivaite crystals and large quartz grains could indicate limited firing time, which would prohibit the development of large cuprorivaite crystals, similarly to what was suggested by Delamare et al. for the Pompeian samples [55]. By decreasing the firing time, the craftspeople could be able to produce a lighter blue pigment at a lower cost [55].

Furthermore, a cluster (145 μm across) of fine-grained white material composed of Si-rich particles with sizes ranging from 1 to 10 μm was observed in Sample 17 (Figure 17). Under the optical microscope, the cluster of these small particles enhances the scattering of light and, therefore, increases the lightness of the pigment. The presence of fine-grained Si-rich particles could be either attributed to a synthetic by-product or to a residue of the starting materials. In the latter case, it would suggest the addition of fine-grained silica, which would increase the total surface of the silica particles and thus optimise the synthesis of cuprorivaite for low-alkali starting mixtures [49,55]. Finally, the intentional addition of a white substance to achieve lighter tones cannot be excluded, since the practice of adding white pigments to Egyptian blue has been documented in raw pigment pellets and applied paint layers from other archaeological settings [2,23,55].

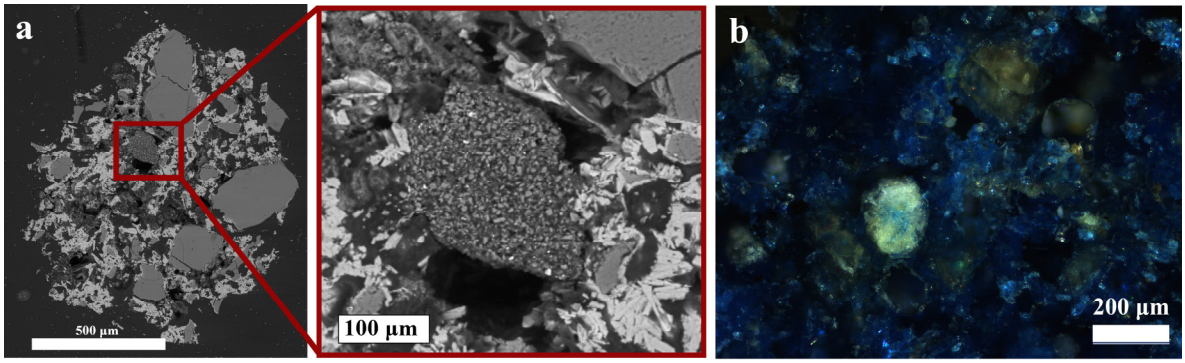

Figure 17. (**a**) Sample 17 has angular to subangular quartz grains with sizes ranging from 15 to 418 μm. The limited size of the cuprorivaite crystals (8 to 62 μm) and agglomerates (25 to 150 μm) is responsible for the lighter tone of the pellet. A cluster of fine-grained Si-rich particles (1 to 10 μm across) is observed. (**b**) Fine-grained agglomerate of Si-rich particles scatters the incident light under observation with the OM.

The results, therefore, illustrate two different methods of production for blue pigments of lighter tones. The first, indicated by the study of Sample 13, included the grinding of the initially produced Egyptian blue pellet to a fine powder and the addition of a cobalt-rich material, possibly to enhance the saturation of the colour. The second method is suggested from the examination of Sample 17, included the firing of the starting materials for the production of Egyptian blue in a shorter time, resulting in the formation of small cuprorivaite crystals. This method was less demanding in terms of firing and fuel, securing the production of light blue pigment at a lesser cost.

Besides the study of the various qualities of successfully produced Egyptian blue pigments, this study includes the investigation of an unsuccessfully produced pellet. Sample 10 was obtained from the crust of an unsuccessfully produced Egyptian blue pellet (Figure 2). The find was associated with a destroyed fire structure 1 (see FS 1 in Figure 1), where the majority of the Egyptian blue pellets were found [35,36]. The

analysis carried out on this sample by SEM-EDS and micro-Raman spectroscopy (Table 2) did not provide evidence for the presence of cuprorivaite. Instead, copper–silicate platy and needle-shaped green crystals were observed by optical microscopy and were identified as chrysocolla ($Cu_4H_4[Si_4O_{10}](OH)_8 \cdot nH_2O$) by Raman spectroscopy (Figure 18). The formation of chrysocolla is most likely the outcome of insufficient quantities of calcium in the starting mixture, at least on the surface from where the sample was obtained. However, since Sample 10 was obtained from the surface crust of an unsuccessful pellet, it cannot provide information about the whole. Further research, including the global analysis of unsuccessfully produced pellets with visible-induced luminescence imaging, is required to confirm the absence of cuprorivaite in the sample.

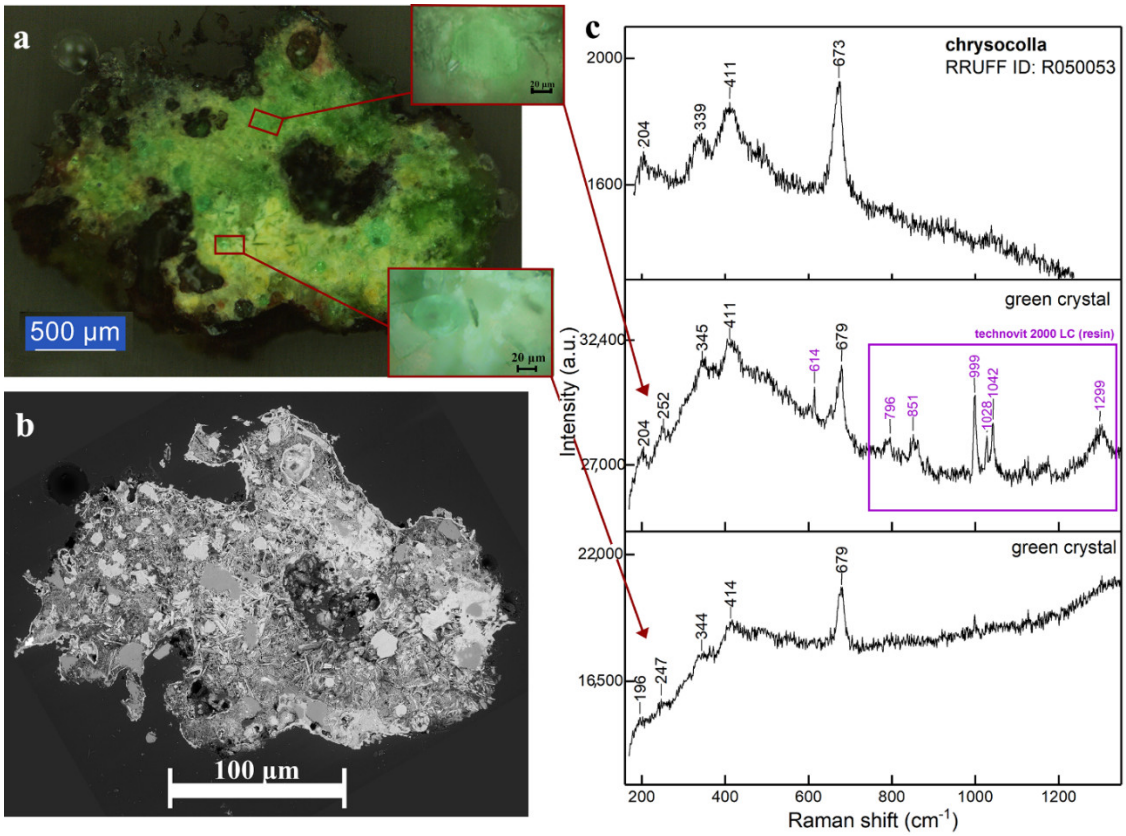

Figure 18. (**a**) Optical micrograph of Sample 10, which was obtained from the surface of an unsuccessfully produced pellet with a dark brown colour. (**b**) BSE micrograph of Sample 10. The EDS analysis showed that copper-rich silicates of green colour are formed in a heterogeneous matrix of quartz and glassy phases. (**c**) The green copper-silicate crystals were characterised as chrysocolla ($Cu_4H_4[Si_4O_{10}](OH)_8 \cdot nH2O$) by Raman spectroscopy. No cuprorivaite particles were detected in the sample by Raman spectroscopy.

4. Conclusions

The examination of the Egyptian blue samples with microanalytical techniques, including optical microscopy, SEM-EDS, and micro-Raman spectroscopy, illustrates the complex technological processes employed for the production of blue pigments carried out in the Koan workshop. The micromorphology of the samples indicates a solid-state production process with a low alkali content in the starting mixture. The use of a low-alkali starting mixture is considered characteristic of Egyptian blue produced in the Hellenistic and Roman periods [49]. When it comes to the use of starting materials, the morphology of the residual quartz particles, as well as the presence of iron and titanium impurities, indicates the use of beach

sand as a silica source. The presence of tin possibly suggests the use of bronze alloys as a copper source. The traces of various metals, including lead and gold, could reflect the intertwined relationship between the different activities carried out in the Koan workshop, i.e., metallurgy and pigment production.

The micromorphology of the samples illustrates the various production steps of the operational sequence. The study of Sample 7 indicates more than one firing stage, while the darker tone of certain pellets could be attributed to the presence of tenorite, pointing to inadequate air supply during firing. Moreover, further processing of the initially produced Egyptian blue pellets to manufacture different tones of blue is documented. The tone of the final product is related not only to the size of the cuprorivaite crystals but also to the size of the cuprorivaite agglomerates. The identification of two different treatment techniques for the creation of a lighter blue pigment, as indicated by Samples 13 and 17, illustrates the high level of technical knowledge of the Koan craftspeople.

Future research, including the colorimetric study of the Egyptian blue pellets of the Koan workshop, would quantitatively illustrate the relationship between the observed colour and the chemical composition of the pellets. Experimental reconstructions of the production processes utilising locally available starting materials and copper alloy filings are required to improve our understanding of the technological processes of Egyptian blue production carried out on Kos. Finally, further research is required to understand the reasons that led to the unsuccessful productions of Egyptian blue.

Author Contributions: Conceptualization, A.K.M.; methodology, A.K.M; software, A.K.M and F.A.; investigation, A.K.M., F.A., C.S.; data curation, A.K.M and F.A.; writing—original draft preparation, A.K.M.; writing—review and editing, A.K.M, F.A., C.S., and S.H.; visualization, A.K.M. All authors have read and agreed to the published version of the manuscript.

Funding: This research received no external funding.

Acknowledgments: We thank the Ephorate of Antiquities of Dodecanese, and especially Mania Michailidou, for supporting the study of the material. Moreover, we would like to thank the Directorate of Conservation of Ancient and Modern Monuments of the Greek Ministry of Culture for permitting the documentation, sampling, and analysis of the finds. We would also like to thank the anonymous peer reviewers for their excellent comments and suggestions. Finally, we want to thank Mncedisi Siteleki for making the map in Figure 11.

Conflicts of Interest: The authors declare no conflicts of interest.

Appendix A

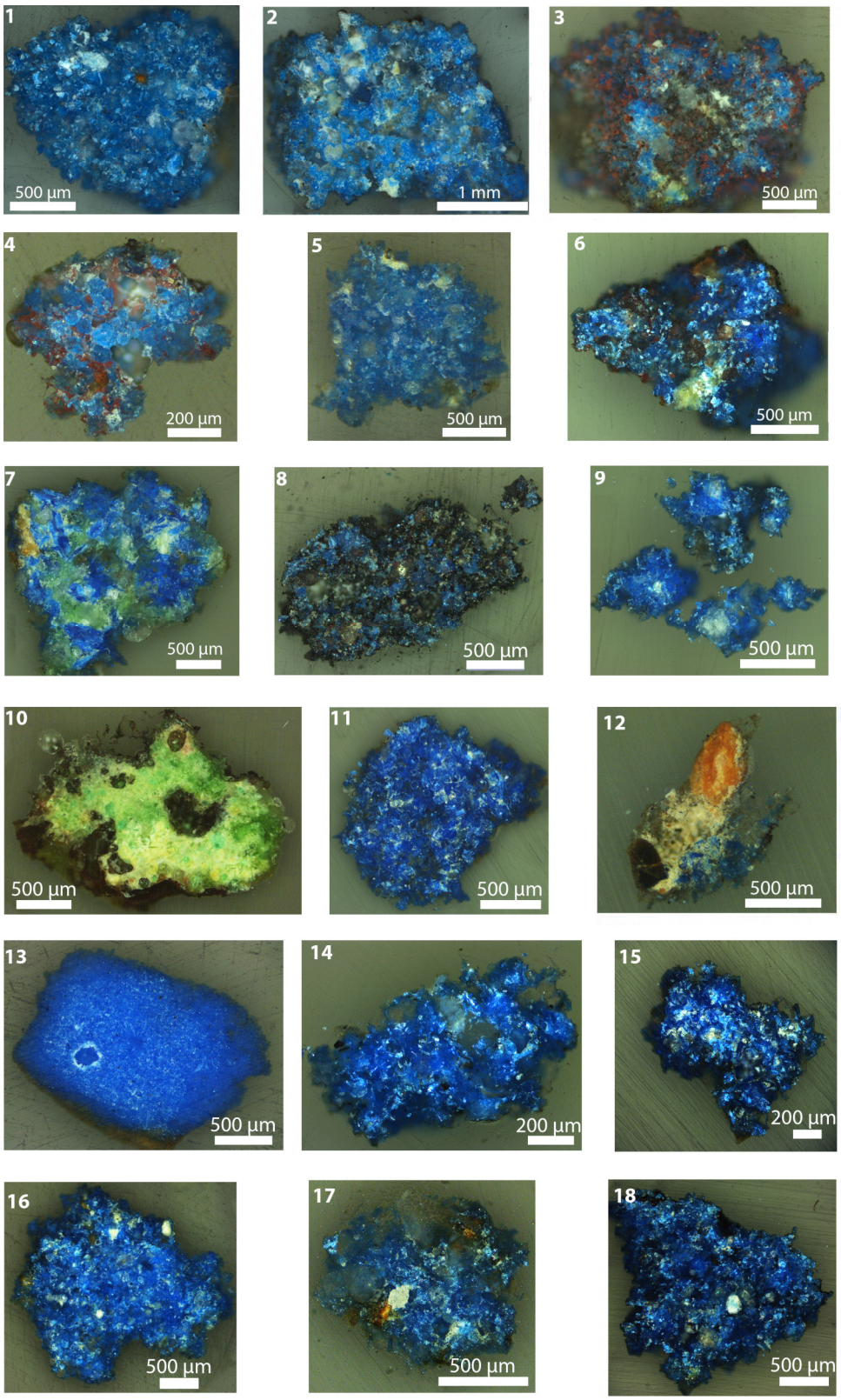

Figure A1. Optical micrographs of the embedded Egyptian blue samples.

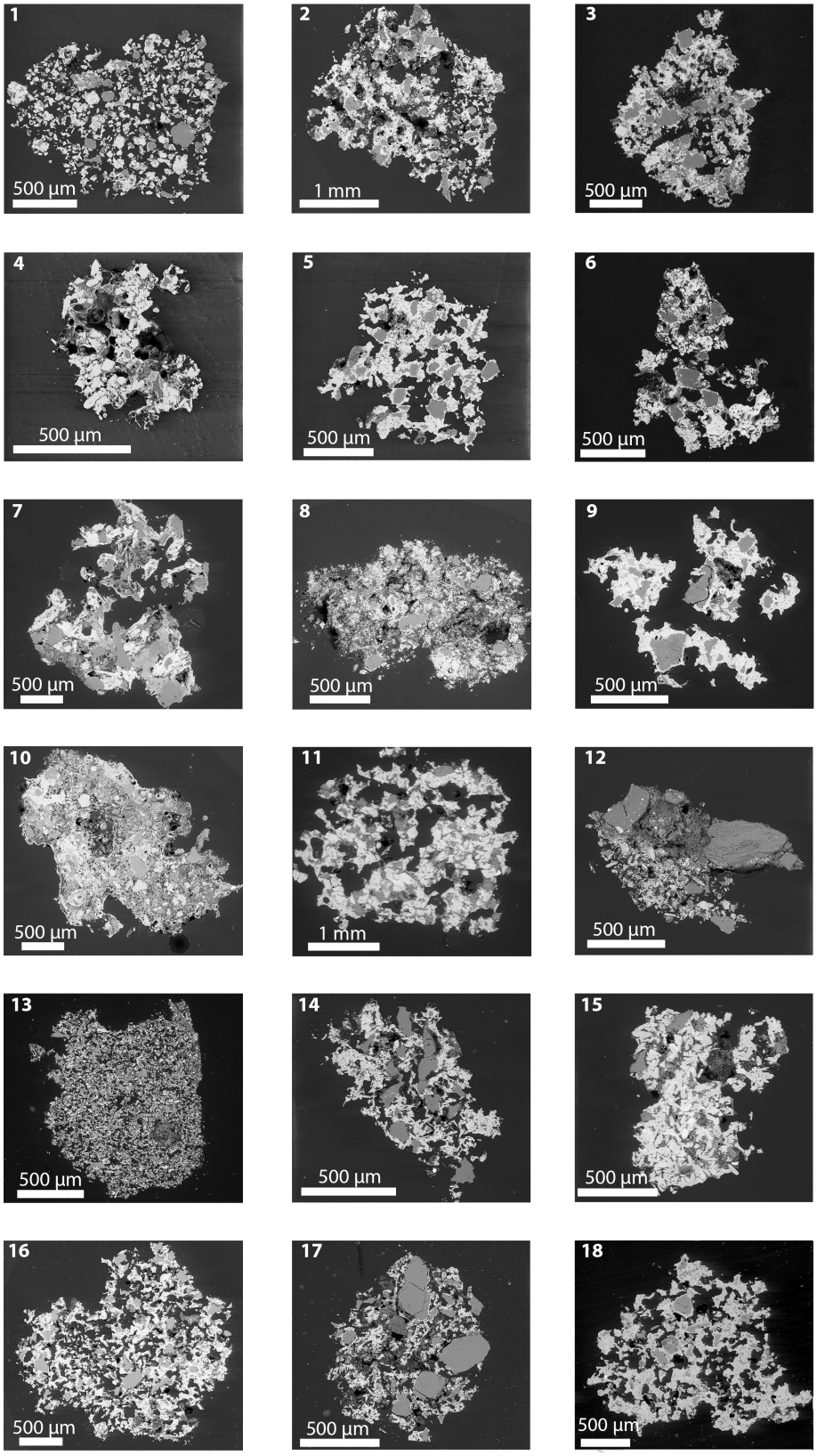

Figure A2. Backscattered electron micrographs of the embedded Egyptian blue samples.

Appendix B

Table A1. Cuprorivaite and quartz particle sizes and cuprorivaite agglomerate sizes. The particles were measured in the maximum dimension. The number of particles measured for each sample was determined by the presence of particles with clearly observable edges in each sample.

	Cuprorivaite					Quartz					Cuprorivaite Agglomerates				
Sample	**No. of Particles Measured**	**Mean**	**SD**	**Min**	**Max**	**No. of Particles Measured**	**Mean**	**SD**	**Min**	**Max**	**No. of Agglomerates Measured**	**Mean**	**SD**	**Min**	**Max**
1	100	34	14	14	72	58	51	30	16	185	7	123	40	71	184
2	101	37	16	15	101	51	99	66	24	371	9	325	144	137	537
3	70	37	13	16	76	33	89	51	29	207	5	228	84	135	349
4	71	26	16	8	85	4	46	25	28	83	5	132	58	71	222
5	100	29	10	10	62	34	69	38	17	157	10	148	60	79	255
6	183	31	14	10	96	12	80	41	33	166	10	221	109	69	369
7	41	119	53	55	258	30	134	98	23	528	4	514	66	417	561
8	92	27	12	10	84	25	71	57	17	232	10	150	71	56	272
9	100	29	10	10	66	15	97	79	21	267	10	186	99	105	424
10						15	108	51	59	246	0				
11	100	111	42	25	221	25	117	47	30	256	11	470	192	219	807
12	35	34	21	11	83	5	56	29	34	104	2	91	7	86	96
13	211	15	7	3	43	55	30	22	10	143	0				
14	100	27	12	8	80	15	92	47	21	181	10	111	76	47	299
15	100	59	24	27	137	10	75	50	19	167	10	189	47	112	257
16	126	41	17	16	105	46	91	43	21	259	11	193	47	117	252
17	100	21	10	8	62	30	88	89	15	418	12	77	30	32	130
18	95	50	16	22	92	15	109	45	32	192	15	308	123	154	575

Table A2. Semiquantitative presentation of the different phases present in each sample expressed as areas %, including residual quartz, cuprorivaite, and the glassy phase. The measurements were carried out using the threshold tool of Fiji (ImageJ) software, and the minimum and maximum threshold for each phase are presented. The areas normalised to the total measured area, excluding the resin, show the extent of overlapping of the different phases.

Sample	Phase	%Area	MinThr	MaxThr	Normalised
1	Quartz	16.75	80	181	45.5
	Cuprorivaite	12.94	221	255	35.1
	Glass	7.16	182	220	19.4
	Total area without resin	36.85	80	255	100.0
2	Quartz	17.78	69	105	43.9
	Cuprorivaite	22.33	106	255	55.1
	Total area without resin	40.51	68	255	99.0
3	Quartz	19.72	72	100	56.0
	Cuprorivaite	15.68	100	138	44.5
	Cu-particles	0.26	139	255	0.7
	Total area without resin	35.22	71	255	101.2
4	Quartz	6.86	100	115	21.5
	Cuprorivaite	18.63	133	255	58.4
	Glassy phase	6.03	116	132	18.9
	Total area without resin	31.91	99	255	98.8
5	Quartz	13.41	77	110	35.1
	Cuprorivaite	19.17	126	255	50.2
	Glassy phase	5.43	111	125	14.2
	Total area without resin	38.17	76	255	99.6
6	Quartz	12.37	57	83	38.1
	Cuprorivaite	16.35	97	255	50.4
	Glassy phase	3.74	84	96	11.5
	Total area without resin	32.46	57	255	100.0
7	Quartz	19.21	76	107	52.7
	Cuprorivaite	10.69	120	255	29.4
	Glassy phase	6.21	108	119	17.1
	Total area without resin	36.42	75	255	99.1
8	Quartz	13.56	145	183	27.3
	Cuprorivaite	10.58	209	255	21.3
	Glassy phase	6.48	184	208	13.1
	Carbon	19.57	85	145	39.4
	Total area without resin	49.63	85	255	101.1
9	Quartz	8.26	82	101	28.7
	Cu-particles	0.02	145	255	0.1
	Cuprorivaite	15.75	116	144	54.8
	Glassy phase	4.59	102	115	16.0
	Total area without resin	28.76	81	255	99.5
10	Quartz	23.44	107	170	56.5
	Cu-Si crystals	3.75	212	255	9.0
	Glassy phase	13.99	171	211	33.7
	Total area without resin	41.46	106	255	99.3
11	Quartz	17.86	60	97	41.3
	Cuprorivaite	25	98	142	57.8
	Sn particles	0.13	142	255	0.3
	Total area without resin	43.27	59	255	99.4

12	Quartz and soil particles	25.01	70	110	88.4
	Cuprorivaite	4.85	111	152	17.1
	Total area without resin	28.29	73	255	105.5
13	Quartz	7.82	106	127	43.5
	Cuprorivaite	9.88	129	255	54.9
	Total area without resin	17.99	106	255	98.4
14	Quartz	17.43	55	92	49.5
	Cuprorivaite	14.47	105	140	41.1
	Sn particles	0.14	140	255	0.4
	Glassy phase	3.19	93	104	9.1
	Total area without resin	35.21	55	255	100.1
15	Quartz	12.56	50	87	40.7
	Cuprorivaite	17.88	88	120	58.0
	Sn particles	0.11	121	255	0.4
	Total area without resin	30.85	49	255	99.0
16	Quartz	14.07	94	154	46.1
	Cuprorivaite	16.27	155	239	53.3
	Sn particles	0.16	240	255	0.5
	Total area without resin	30.5	94	255	100.0
17	Quartz	18.59	130	159	56.7
	Cuprorivaite	14.2	160	255	43.3
	Total area without resin	32.79	130	255	100.0
18	Quartz	13.8	97	161	38.5
	Cuprorivaite	22.29	161	210	62.2
	Sn particles	0.06	211	255	0.2
	Total area without resin	35.85	97	255	100.8

References

1. Delamare, F. Egyptian blue, the blue pigment of Mediterranean antiquity: from Egyptian *hsbḏ iryt* to Roman *caeruleum*. In *Blue Pigments: 5000 Years of Art and Industry*; Archetype Publications: London, UK, 2013; pp. 1–36.
2. Kakoulli, I. Egyptian blue in Greek painting between 2500 and 50 BC. In *From Mine to Microscope: Advances in the Study of Ancient Technology*; Shortland, A., Freestone, I., Rehren, T., Eds.; Oxbow Books: Oxford, UK, 2009; pp. 79–92.
3. Berke, H. The invention of blue and purple pigments in ancient times. *Chem. Soc. Rev.* **2007**, *36*, 15–30.
4. Delamare, F. German azurite and English blue verditer. In *Blue Pigments: 5000 Years of Art and Industry*; Archetype Publications: London, UK, 2013; pp. 119–144.
5. Riederer, J. Egyptian blue. In *Artists' Pigments: A Handbook of Their History and Characteristics*; FitzHugh, E.W., Eds; National Gallery of Art: Washington, DC, USA, 1997; Volume 3, pp. 23–46.
6. Ullrich, D. Egyptian blue and green frit: Characterization, history and occurrence, synthesis. In *Datation-Characterisation des Peintures Parietales and Murales,* PACT: Ravello, Italy, 1987; pp. 323–332.
7. Caley, E.R.; Richards, J.F. *Theophrastus: On Stones, Introduction, Greek Text, English Translation, and Commentary*; The Ohio State University: Columbus, OH, USA, 1956.
8. Filippakis, S.E.; Perdikatsis, B.; Paradellis, T. An analysis of blue pigments from the Greek Bronze Age. *Stud. Conserv.* **1976**, *21*, 143–153.
9. Profi, S.; Weier, L.; Filippakis, S. X-ray analysis of Greek Bronze Age pigments from Knossos. *Stud. Conserv.* **1976**, *21*, 34–39.
10. Profi, S.; Weier, L.; Filippakis, S. X-ray analysis of Greek Bronze Age pigments from Mycenae. *Stud. Conserv.* **1974**, *19*, 105–112.
11. Panagiotaki, M.; Tite, M.S.; Maniatis, Y. Egyptian blue in Egypt and beyond: The Aegean and the Near East. In *Proceedings of the Tenth International Congress of Egyptologists*, *University of the Aegean, Rhodes, Greece 22–29 May 2008*; Kousoulis, P., Lazaridis, N., Eds.; Peeters: Leuven, Belgium; Paris, France; Bristol, UK, 2015; Volume II, pp. 1769–1789.
12. Pantermalis, D.; Vlassopoulou, C.; Katsaros, T.; Panagiotidou, D.; Merkouri, E.; Kokkinou, L. *Archaic Colors*; Acropolis Museum: Athens, Greece, 2012.
13. Kouzeli, K.; Beloyannis, N.; Dogani, Y. Study of remaining colour on the architectural surfaces of the Parthenon. In *Proceedings of the Superfici dell' Architettura: Le Finiture. Atti del convegno di studi Bressanone, Bressanone, Italy, 26–29 June 1990*; Biscontin, G., Eds.; Libreria Progetto: Bressanone, Italy, 1990; pp. 241–250.
14. Brecoulaki, H. *La Peinture Funéraire de Macédoine: Emplois et Fonctions de La Couleur (IVe–IIe s. av. J. –C.)*; Centre de recherches de l'antiquité grecque et romaine, Fondation nationale de la recherche scientifique: Athens, Greece, 2006.
15. Brecoulaki, H.; Fiorin, E.; Vigato, P.A. The funerary klinai of tomb 1 from Amphipolis and a sarcophagus from ancient Tragilos, eastern Macedonia: A physico-chemical investigation on the painting materials. *Cult. Herit.* **2006**, *7*, 301–311.
16. Bordignon, F.; Postorino, P.; Dore, P.; Trojsi, G. Raman identification of green and blue pigments in Etruscan polychromes on architectural terracotta panels. *J. Raman Spectrosc.* **2007**, *38*, 255–259.
17. Tite, M.S.; Hatton, G.D. The production technology of, and trade in, Egyptian blue pigment in the Roman world. In *Communities and Connections: Essays in Honour of Barry Cunliffe*; Oxford University Press: Oxford, UK, 2007; pp. 75–92.
18. Béarat, H. Quelle est la gamme exacte des pigments Romains? Confrontation des resultats d'analyse et des textes de Vitruve et de Pline. In *Proceedings of the International Workshop, Fribourg, Switzerland, 7–9 March 1996*; Béarat, H., Fuchs, M., Maggetti, M., Paunier, D., Eds.; Institute of Mineralogy and Petrography: Fribourg, Switzerland, 1997; pp. 11–34.
19. Mateos, L.D.; Cosano, D.; Mora, M.; Muñiz, I.; Carmona, R.; Jiménez-Sanchidrián, C.; Ruiz, J.R. Raman microspectroscopic analysis of decorative pigments from the Roman villa of El Ruedo (Almedinilla, Spain). *Spectrochim. Acta Part A Mol. Biomol. Spectrosc* **2015**, *151*, 16–21.

20. Duran, A.; Jimenez De Haro, M.C.; Perez-Rodriguez, J.L.; Franquelo, M.L.; Herrera, L.K.; Justo, A. Determination of pigments and binders in Pompeian wall paintings using Synchrotron Radiation—High-resolution X-ray powder diffraction and conventional spectroscopy—Chromatography. *Archaeometry* **2010**, *52*, 286–307.
21. Aliatis, I.; Bersani, D.; Campani, E.; Casoli, A.; Lottici, P.P.; Mantovan, S.; Marino, I.G. Pigments used in Roman wall paintings in the Vesuvian area. *J. Raman Spectrosc.* **2010**, *41*, 1537–1542.
22. Delaney, J.K.; Dooley, K.A.; Radpour, R.; Kakoulli, I. Macroscale multimodal imaging reveals ancient painting production technology and the vogue in Greco-Roman Egypt. *Sci. Rep.* **2017**, *7*, 15509.
23. Radpour, R.; Fischer, C.; Kakoulli, I. New Insight into Hellenistic and Roman Cypriot Wall Paintings: An Exploration of Artists' Materials, Production Technology, and Technical Style. *Arts* **2019**, *8*, 74.
24. Kakoulli, I. Roman Wall Paintings in Cyprus: a Scientific Investigation of their Technology. In *Proceedings of the International Workshop on Roman Wall Painting, Fribourg, Switzerland, 7–9 March 1996*; Béarat, H., Fuchs, M., Maggetti, M., Paunier, D., Eds.; Institute of Mineralogy and Petrology, Fribourg University: Fribourg, Switzerland, 1997.
25. Augusti, S. *I Colori Pompeiani*; De Luca Editore: Rome, Italy, 1967.
26. Rosenqvist, A.M. Analyser av sverd og skjold fra Bø-funnet. *Viking* **1959**, *23*, 29–34.
27. Tite, M.S.; Bimson, M.; Cowell, M.R. Technological examination of Egyptian blue. In *Archaeological Chemistry-III*; American Chemical Society: Washington, DC, USA, 1984; pp. 215–242.
28. Boschetti, C. Vitreous materials in early mosaics in Italy: Faience, Egyptian blue, and glass. *J. Glass Studies* **2011**, *53*, 59–91.
29. Cavassa, L. La production du bleu égyptien durant l'époque hellenistique et l'Empire romain (III s.av. J.-C.-I s. apr. J.-C.). In *Bulletin de Correspondance Hellénique. Supplément. Les arts de la couleur en Gréce ancienne… et ailleurs. Approches interdisciplinaires*; Jockey, P., Eds.; École Française d' Athènes: Athens, Greece, 2018; Volume 56, pp. 13–34.
30. Petrie, W.M.F.; Walker, J.H. *Memphis I*; School of Archaeology in Egypt University College: London, UK, 1909.
31. Nicholson, P.T. *Working in Memphis: The Production of Faience at Roman Period Kom Helul*; Egypt Exploration Society: London, UK, 2013.
32. Cavassa, L.; Delamare, F.; Repoux, M. La fabrication du bleu égyptien dans les champs phlégréens (Campanie, Italie) durant le I^{er} siècle de notre ère. *Aspects de l'artisanat en milieu urbain: Gaule et Occident romain, Suppléments à la Revue archéologique de l'Est* **2010**, *28*, 235–249.
33. Lazzarini, L.; Verità, M. First evidence for 1st century AD production of Egyptian blue frit in Roman Italy. *J. Archaeol. Sci.* **2015**, *53*, 578–585.
34. Grifa, C.; Cavassa, L.; Bonis, A.D.; Germinario, C.; Guarino, V.; Izzo, F.; Kakoulli, I.; Langella, A.; Mercurio, M.; Morra, V. Beyond Vitruvius: New insight in the technology of Egyptian blue and green frits. *J. Am. Ceram. Soc.* **2016**, *99*, 3467–3475.
35. Kantzia, C.; Kouzeli, K. Workshop for the manufacture of pigments in the ancient Agora of Kos [original title: Το εργαστήριο παρασκευής χρωμάτων στην Αρχαία Αγορά της Κω: Το Αιγυπτιακό μπλε]. *Athens Ann. Archaeol.* **1991**, *20*, 210–250.
36. Kostomitsopoulou Marketou, A. The Pigment Production Site of the Ancient Agora of Kos (Greece): Revisiting the material evidence. *Thiasos J. Archaeol. Anc. Archit.* **2019**, *8*, 61–80.
37. Kostomitsopoulou Marketou, A.; Kouzeli, K.; Facorellis, Y. Colourful earth: Iron-containing pigments from the Hellenistic pigment production site of the ancient agora of Kos (Greece). *J. Archaeol. Sci. Rep.* **2019**, *26*, 101843.
38. Berke, H. Chemistry in ancient times: The development of blue and purple pigments. *Angew. Chemie Int. Ed.* **2002**, *41*, 2483–2487.
39. Chase, W.T. Egyptian blue as a pigment and ceramic material. In *Science and Archaeology*; Brill, R.H., Eds.; MIT Press: Cambridge, MA, USA, 1971; pp. 80–90.
40. Wiedemann, H.G.; Bayer, G. The bust of Nefertiti. *Anal. Chem.* **1982**, *54*, 619–628.
41. Jaksch, H.; Seipel, W.; Weiner, K.L.; El Goresy, A. Egyptian blue—Cuprorivaite a window to ancient Egyptian technology. *Nature* **1983**, *70*, 525–535.

42. Bianchetti, P.; Talarico, F.; Vigliano, M.G.; Ali, M.F. Production and characterization of Egyptian blue and Egyptian green frit. *J. Cult. Herit.* **2000**, *1*, 179–188.
43. Bouherour, S.; Berke, H.; Wiedemann, H.-G. Ancient man-made copper silicate pigments studied by Raman microscopy. *Chim. Int. J. Chem.* **2001**, *55*, 942–951.
44. Pagès-Camagna, S.; Colinart, S.; Coupry, C. Fabrication processes of archaeological Egyptian blue and green pigments enlightened by Raman microscopy and scanning electron microscopy. *J. Raman Spectrosc.* **1999**, *30*, 313–317.
45. Pagès-Camagna, S.; Reiche, I.; Brouder, C.; Cabaret, D.; Rossano, S.; Kanngießer, B.; Erko, A. New insights into the colour origin of archaeological Egyptian blue and green by XAFS at the Cu K-edge. *X-Ray Spectrom.* **2006**, *35*, 141–145.
46. Pagès-Camagna, S.; Colinart, S. The Egyptian green pigment: Its manufacturing process and links to Egyptian blue*. *Archaeometry* **2003**, *45*, 637–658.
47. Pradell, T.; Salvado, N.; Hatton, G.D.; Tite, M.S. Physical processes involved in production of the ancient pigment, Egyptian Blue. *J. Am. Ceram. Soc.* **2006**, *89*, 1426–1431.
48. Hatton, G.D.; Shortland, A.J.; Tite, M.S. The production technology of Egyptian blue and green frits from second millennium BC Egypt and Mesopotamia. *J. Archaeol. Sci.* **2008**, *35*, 1591–1604.
49. Delamare, F. Sur les processus physiques intervenant lors de la synthèse du bleu égyptien. *ArchéoSciences, Revue d'Archéométrie* **1997**, 21, 103–119.
50. Schiegl, S.; Weiner, K.L.; El Goresy, A. Zusammensetzung und Provenienz von blau-und grünpigmenten in altägyptischen Wandmalereien: ein Beitrag zur exakten Chronologie der Bronzetechnologie in Altägypten. *Erzmetall* **1990**, *43*, 265–272.
51. Pozza, G.; Ajò, D.; Chiari, G.; De Zuane, F.; Favaro, M. Photoluminescence of the inorganic pigments Egyptian blue, Han blue and Han purple. *J. Cult. Herit.* **2000**, *1*, 393–398.
52. Pabst, A. Structures of some tetragonal sheet silicates. *Acta Crystallogr.* **1959**, *12*, 733–739.
53. Mazzi, F.; Pabst, A. Re-examination of cuprorivaite. *Am. Mineral.* **1962**, *47*, 409–411.
54. Bensch, W.; Schur, M. Crystal structure of calcium copper phyllo-decaoxotetrasilicate, $CaCuSi_4O_{10}$. *Z. für Kristallographie Cryst. Mater.* **1995**, *210*, 530.
55. Delamare, F.; Monge, G.; Repoux, M. À la recherche de différentes qualités marchandes dans les bleus égyptiens trouvés à Pompéi. *Rivista di Studi Pompeiani* **2004**, *XV*, 89–107.
56. Pliny the Elder. *Natural History, Books 33–35, with an English Translation by H. Rackham*; Harvard University Press: Cambridge, MA, USA, 1968; Volume IX.
57. Vitruvius, M.V.P. *On Architecture, Books 6–10, Edited and Translated by Frank Granger*; Harvard University Press: Cambridge, MA, USA, 1934; Volume II.
58. Schindelin, J.; Arganda-Carreras, I.; Frise, E.; Kaynig, V.; Longair, M.; Pietzsch, T.; Preibisch, S.; Rueden, C.; Saalfeld, S.; Schmid, B., et al. Fiji: an open-source platform for biological-image analysis. *Nat. Methods* **2012**, *9*, 676-682.
59. Schneider, C.A.; Rasband, W.S.; Eliceiri, K.W. NIH Image to ImageJ: 25 years of image analysis. *Nat. Methods* **2012**, *9*, 671-675.
60. Adams, A.E.; MacKenzie, W.S.; Guilford, C. *Atlas of Sedimentary Rocks under the Microscope*; Longman: Harlow, Essex, UK, 1984.
61. Feller, R.L. *Artists' Pigments: A Handbook of their History and Characteristics*; Feller R. L., Eds.; Archetype Publications: London, UK, 1986; Volume 1.
62. Lafuente, B.; Downs, R.T.; Yang, H.; Stone, N. The power of databases: The RRUFF project. In *Highlights in Mineralogical Crystallography*; Armbruster, T., Danisi, R.M., Eds.; De Gruyter: Berlin, Germany, 2015; pp. 1–30.
63. Bruni, S.; Cariati, F.; Casadio, F.; Toniolo, L. Spectrochemical characterization by micro-FTIR spectroscopy of blue pigments in different polychrome works of art. *Vib. Spectrosc.* **1999**, *20*, 15–25.
64. Bell, I.M.; Clark, R.J.H.; Gibbs, P.J. Raman spectroscopic library of natural and synthetic pigments (pre- ≈ 1850 AD). *Spectrochim. Acta Part A Mol. Biomol. Spectrosc.* **1997**, *53*, 2159–2179.

65. Guineau, B.; Gratuze, B.; Blet-Lemarquand, M. Caractérisation de boules de bleu égyptien: Analyse par absorption visible et par activation avec des neutrons rapides de cyclotron. *ArchéoSciences, revue d'Archéométrie* **1997**, *21*, 121–130.
66. Warner, T.E. Artificial cuprorivaite $CaCuSi_4O_{10}$ (Egyptian blue) by a salt-flux method. In *Synthesis, Properties and Mineralogy of Important Inorganic Materials*, Warner, T.E., Ed.; John Wiley & Sons, Ltd.: West Sussex, UK, 2011; pp. 26–49.
67. Stiegeler, S.E. *A Dictionary of Earth Sciences*; Palgrave Macmillan: London, UK, 1976.
68. Giménez, J.; Espriu-Gascon, A.; Bastos-Arrieta, J.; de Pablo, J. Effect of NaCl on the fabrication of the Egyptian blue pigment. *J. Archaeol. Sci. Rep.* **2017**, *14*, 174–180.
69. Nicola, M.; Seymour, L.M.; Aceto, M.; Priola, E.; Gobetto, R.; Masic, A. Late production of Egyptian blue: Synthesis from brass and its characteristics. *Archaeol. Anthropol. Sci.* **2019**, *11*, 5377–5392.
70. Hatton, G.D. The Technology of Egyptian blue. Ph.D. Thesis, University of Oxford, Oxford, UK, 2005.
71. El Goresy, A. Polychromatic wall painting decorations in monuments of Pharaonic Egypt: Compositions, chronology and painting techniques. In *The wall paintings of Thera, Proceedings of the first international symposium, Petros M. Nomikos Conference Centre, Thera, Hellas, 30 August–4 September 1997*; Sherratt, S., Eds.; Petros M. Nomikos and the Thera Foundation: Athens, Greece, 2000; pp. 49–70.
72. Scott, J.F. Raman Spectrum of SnO_2. *J. Chem. Phys.* **1970**, *53*, 852–853.
73. Yang, X.-L.; Wan, X.-X. Analysis of the spectral reflectance and color of mineral pigments affected by their particle size. *Color Res. Appl.* **2020**, *45*, 246–261.
74. Wang, W.H.; Ren, X. Flux growth of high-quality $CoFe_2O_4$ single crystals and their characterization. *J. Cryst. Growth* **2006**, *289*, 605–608.
75. Wang, T.; Zhu, T.; Brunet, M.; Deshayes, C.; Sciau, P. Raman study of Yuan Qinghua porcelain: the highlighting of dendritic $CoFe_2O_4$ crystals in blue decorations. *J. Raman Spectrosc.* **2017**, *48*, 267–270.
76. Shortland, A.J.; Tite, M.S.; Ewart, I. Ancient exploitation and use of cobalt alums from the Western Oases of Egypt. *Archaeom.* **2006**, *48*, 153–168.
77. Shortland, A.J.; Tite, M.S. Technological study of Ptolemaic–Early Roman faience from Memphis, Egypt. *Archaeom.* **2005**, *47*, 31–46.